FLUXATRON AND SONIC ANEMOMETER MEASUREMENTS OF THE MOMENTUM FLUX AT A HEIGHT OF 4 METRES IN THE ATMOSPHERIC BOUNDARY LAYER

by

JOHN WILLIAM MCDONALD

B.Sc., University of Victoria, 1969

A THESIS SUBMITTED IN PARTIAL FULFILLMENT OF THE REQUIREMENTS FOR THE DEGREE OF

MASTER OF SCIENCE

in the Department

of

Physics

and the Institute of Oceanography

We accept this thesis as conforming to the required standard

THE UNIVERSITY OF BRITISH COLUMBIA

January, 1972

ABSTRACT

At the International Comparison of Turbulence Measuring Instruments, 1970, velocity components and momentum flux measurements were compared using propeller-type Fluxatrons (Hicks, 1970) and sonic anemometers from Kaijo-Denki, Japan and the Institute of Atmospheric Physics, U.S.S.R. There were distinct differences found in the measurements of the vertical velocity from the propeller sensors. The propeller's momentum flux measurements computed from its velocity components were also different.

The U' propeller was found to be linear for lower frequencies with an associated distance constant of about 7 metre. Measurement of the variance of U' for $f < 0.16$ hz. showed the U' propeller in excess of both sonics by 20%. However, with the propeller's high frequency loss beyond $f = 0.2$ hz. the discrepancy was reduced to only an 8% excess for $.00055$ hz. $< f < 10.8$ hz.

The W' propeller response was non-linear and had an upper cut-off frequency of 1 hz. Because of its non-linear response and stalling characteristics at low wind speeds and also its high frequency cut-off the W' propeller was observed to measure only about 50% of the total fluctuating W' energy available.

Analysis of the sonic cospectra of momentum showed that significant contributions to the momentum flux were to

be found in the frequency domain 0.001 hz. < f < 5.0 hz. The combined response effects of the propeller were enough to reduce the Fluxatron's estimate of this momentum flux by 32.5%.

TABLE OF CONTENTS

LIST OF TABLES

LIST OF FIGURES

ACKNOWLEDGEMENTS

The writer expresses his indebtedness to his thesis supervisor, Dr. M. Miyake, for helpful suggestions and guidance during the period of study at U.B.C. He also recognizes the efforts of all the students in the Air-Sea Interaction Programme who helped in the processing of the data. The many contributions in both time and advice of Mr. Dominique Rossignol deserves special mention. Also Mr. Don Hume who worked long hours taking data and keeping the electronics working and Miss Daphne Friesen for her help in the analysis.

Drs. A. Dyer and B. Hicks from C.S.I.R.O. of Australia deserve special recognition for their many courtesies and scientific advice during the experiment. Without simultaneous measurements from their Fluxatron to match the sonic outputs this thesis could not have been attempted.

The experiment itself was conducted at the Tsimlyansk Field Station of the Academy of Science of the U.S.S.R. and special thanks and recognition must go to all our Russian colleagues who made the experiment possible. Dr. Obukov, Dr. Tsvang, Dr. Koprov, and Dr. Zubkovsky deserve special thanks.

While working in Graduate Studies at the Institute of Oceanography the author received personal financial support from the National Research Council of Canada.

CHAPTER I

INTRODUCTION

1.1 Previous Work and Purpose of this Study

In the past several years many significant steps have been taken in the area of equipment design for the measurement of atmospheric turbulence. Of most significance recently was the development of the sonic anemometer-thermometer (Bovsherov, 1960 and Mitsuta et al, 1967). The sonic anemometer developed by Mitsuta at Kyoto University in Japan operated on a pulse-type of transmission while the instrument developed by the Institute of Atmospheric Physics, Academy of Science, U.S.S.R. operated on a continuous wave principle. Both types of the sonic anemometer are rather elaborate electronic devices, hence are costly to build and require much time and effort to maintain in proper working order under field conditions.

Meanwhile much useful turbulence data have been obtained in Australia by an instrument using two propeller sensors. It was developed at the Met. Division of C.S.I.R.O. by Dyer et al (1967) and called a Fluxatron. The most recent version (Hicks, 1970) used two Gill anemometers and a wind vane to measure horizontal and vertical components of the wind. A thermistor bead was used to give the associated fluctuations of temperature. This instrument was then capable of multiplying and integrating instantaneously to give the heat and momentum flux. The propeller sensors were very simple in design and, under field conditions, less time consuming to maintain than were the sonic anemometers. The cost of such a system was also much less.

In early comparisons of sonic anemometer measurements the results obtained by different groups frequently revealed some disagreement. This disagreement was thought due to either an improper evaluation of meteorological phenomena or incorrect consideration of the factors affecting calibration and response of the measuring instruments. In order to check the latter there have been several joint intercomparisons since 1966. Miyake et al (1970) and Tsvang et al (1971) were two such ones held at U.B.C.

This thesis was attempted in order to study data obtained from a sonic anemometer and that from a Fluxatron's propellers. Causes, if any, for discrepancies in the horizontal and vertical wind components (U' and W') were to be found in terms of the spectra and cospectra for each of the velocity components.

1.2 Description of Experiment

During the period of June 15 to July 20, 1970, an expedition for the comparison of atmospheric turbulence sensors was conducted at the Tsimlyansk Field Station of the Institute of Atmospheric Physics, U.S.S.R. This particular site was located about 200 miles east of Rostov on the Don River and was where most of the turbulence measurements reported by the I.F.A. groups had been produced in the past fifteen years.

Scientific participants in the experiment came from four different countries. They included Drs. Dyer and Hicks from Australia; Drs. Tsvang, Zubkovsky, Koprov, Perepelkina, Timanovsky, and others from the U.S.S.R.; Drs. Businger, Frenzen and Paulsen from the U.S.A.; and Dr. Miyake and myself from Canada.

There were a vast number of turbulence measuring instruments used and compared during this experiment. All were instruments used in the past to supply the turbulence knowledge we have today. To measure the fluctuating components of the wind field, acoustic anemometers from I.F.A. (U.S.S.R.) and Kaijo-Denki (Japan); Fluxatrons from C.S.I.R.O. (Australia); miniature cup anemometers from Argonne National Lab (U.S.A.); and hot wires from D.I.S.A. (Denmark) were all used. To measure the fluctuation of temperature, the Australians used thermistors, the Russians used fine wire resistance thermometers, and the U.B.C. group used acoustic anemometer-thermometers from Kaijo-Denki. The fluctuations of humidity were measured by the U.B.C. group using an ultraviolet Lyman-Alpha humidiometer and by the Russian group using an infrared humidiometer.

The actual experimentation was conducted on a relatively even section of the Russian Steppes with a slope of 1/100 in its southwest part. The area was of dimension 600 by 900 metres covered with short grass and surrounded by an arable part of the steppes planted with clover and corn. To the south-east a uniformly uncultivated part of the steppes extended out some 1500 metres from the measurement area. Since this was the direction of the prevailing wind for June and July all the measurements were made with relatively good fetch conditions.

A rough sketch of the site is shown in Figure 1. All recording equipment other than sensor heads were located in an underground bunker about 30 metres downwind from the main mast. The I.F.A. group based their own equipment some 50 metres downstream from the mast on a truck. Another smaller underground bunker was used for profile measurements of the University of Washington and I.F.A.

The base camp was located about 500 metres away where a cafeteria, recreational facilities, computer centre, work houses, and sleeping area could be found. The entire site was thought to be an adequate location to both measure, record, and analyze turbulent atmospheric data, especially for the intercomparison of sensors when surface horizontal homogeneity is not so important.

Figure 2 gives a pictorial view of the sonic anemometers (Kaijo-Denki and I.F.A.) as they were used in the field. On the far right of the mast the 20 cm. sound path Kaijo-Denki sonic anemometer was mounted. There were three pairs of sound paths used to determine all wind components. One of the pairs was mounted vertically and the other two in a

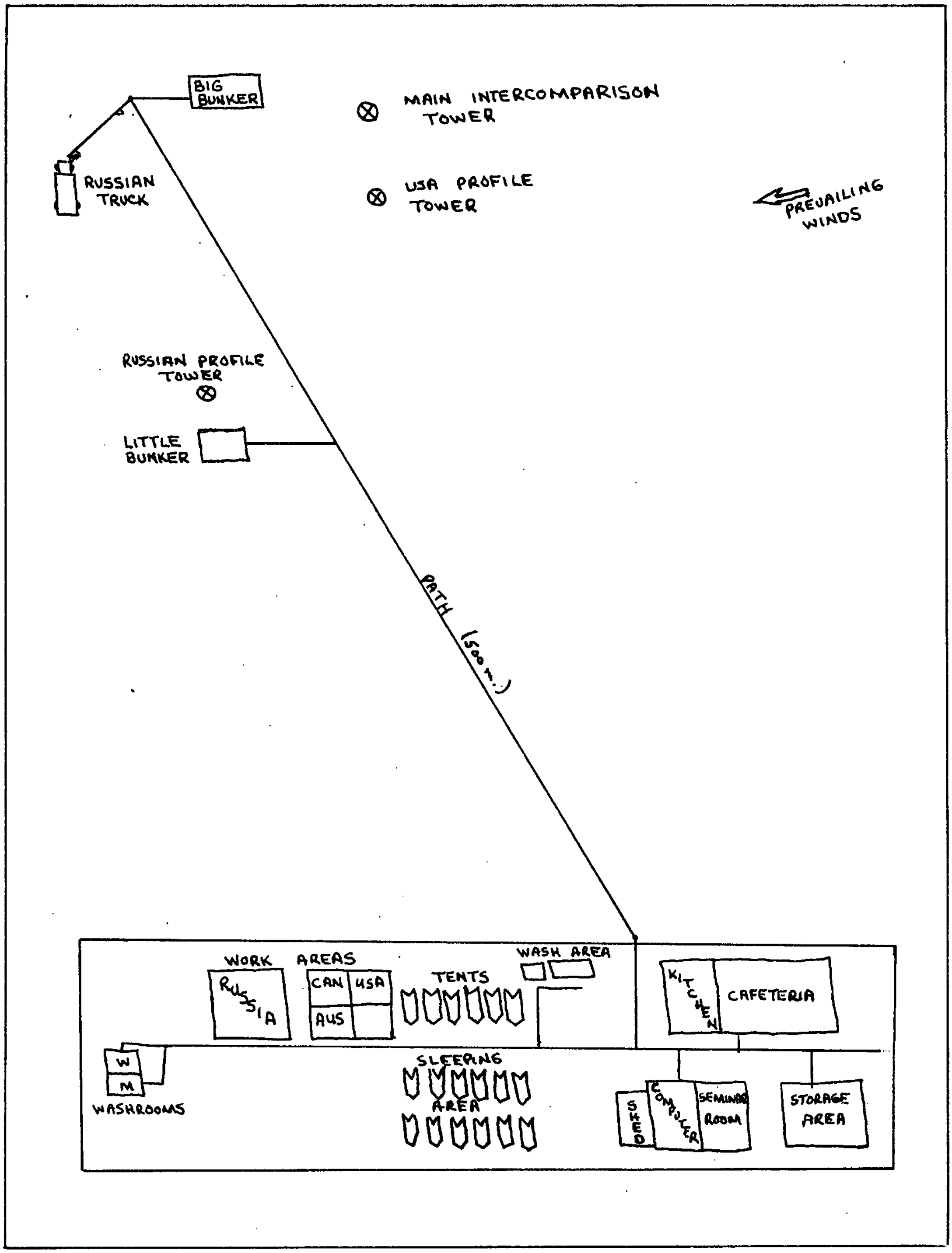

FIGURE #1. SITE DIAGRAM

FIGURE 2

horizontal plane (the horizontal paths were separated 120° to avoid structural interference). The path length limited the wave number resolution of the sonic anemometer to scale sizes of about 1 metre. Each pair contained two sets of transmission and receiving transducers, one set transmitting one way and the other set the reverse direction. Since both transmitted at the same time, the difference of the two transit times gave an absolute measure of the velocity fluctuation. The sum of the two gave an indication of the instantaneous sound speed in air and thus the temperature, assuming the speed of sound depends mainly on the temperature, and not the humidity.

On the left of Figure 2 are two I.F.A. sensors each containing 1 transducer for transmission (the centre one), 3 transducers for receiving (2 upper ones for U' and 2 outer ones for W'), and a fine wire array for measuring temperature. The I.F.A. sensors did not have any provision to measure the V' component of the wind.

The Fluxatron, as used by the Australian group, is shown in Figure 3. Two such devices were used during the expedition in order to measure spatial variability of the momentum flux and heat flux (Dyer and Hicks, 1970). The basic design was simple. Two propeller (Gill type) anemometers and a vane were used for measuring vertical and total horizontal velocity components. Temperature fluctuations were detected by a small thermistor bead. Long time constant R-C filters were employed to remove both the mean levels and

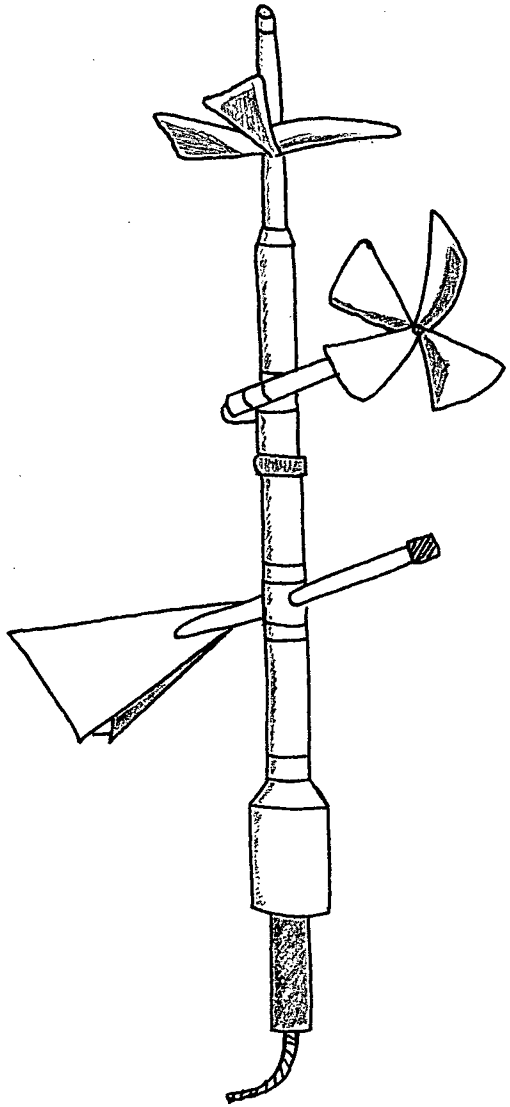

FIGURE 3 - THE FLUXATRON

the long period fluctuations. Internal electronics generated a constant voltage output of two square wave signals which were used to calibrate the fluctuations of the longitudinal and vertical velocity components when the data was played back.

For the experimental data used in this thesis one of the Russian sonics in Figure 2 was replaced with the Fluxatron in an attempt to make a three way intercomparison with the smallest spatial separation.

The data were gathered during the period June 23 to July 21, 1970. Each recorded tape was designated with a T (for Tsimlyansk) and then a 3 digit numeral to indicate which run. For this study three separate cases were analyzed in detail. One case was from measurements on June 29 and two cases were from measurements on July 5. The run on June 29 was designated as T013 while the runs on July 5 were designated T026 and T029 respectively. Run T013 began at 21:36 and ended at 22:08 L.S.T.; Run T026 began at 10:30 and ended at 11:10 L.S.T.; and Run T029 began at 16:45 and ended at 17:17 L.S.T.

CHAPTER 2

ANALYSIS PROCEDURES

2.1 Data Recording

The electrical signals from each sensor were recorded in a frequency modulated form using a bank of 12 voltage controlled oscillators. The characteristics of each oscillator are shown in table 1. Each channel was alligned so that a $\pm$ 1.00 volt input corresponded to an output of $\pm$ 7.5% frequency deviation from the centre frequency of that particular channel. The frequency output increases as the input voltage changes in a positive direction. All the channel outputs were then multiplexed and recorded on one direct record channel of a Hewlett Packard tape recorder. The tapes were then shipped back to Vancouver for analysis.

2.2 Spectral Analysis

At U.B.C. the multiplexed signal was passed through a 12 channel discriminator network which reconverted the data back to original condition. Then signals were digitized on an A-D converter.

Figure 4 shows a block diagram of the U.B.C. spectral processing scheme. The full scale voltage level present at the Analogue to Digital Converter is changed to a 10 bit binary number. This means the full scale voltage is quantized into 1024 (2^{10}) levels.

Table 1

V.C.O. CHARACTERISTICS

±7.5% CHANNELS

Channel	Center Freq. (c/s)	Lower Deviation Limit (c/s)	Upper Deviation Limit (c/s)	Nom. Freq. Response (c/s)
1	400	370	430	6
2	560	518	602	8
3	730	675	785	11
4	960	888	1,032	14
5	1,300	1,202	1,398	20
6	1,700	1,572	1,828	25
7	2,300	2,127	2,473	35
8	3,000	2,775	3,225	45
9	3,900	3,607	4,193	59
10	5,400	4,995	5,805	81
11	7,350	6,799	7,901	110
12	10,500	9,712	11,288	160

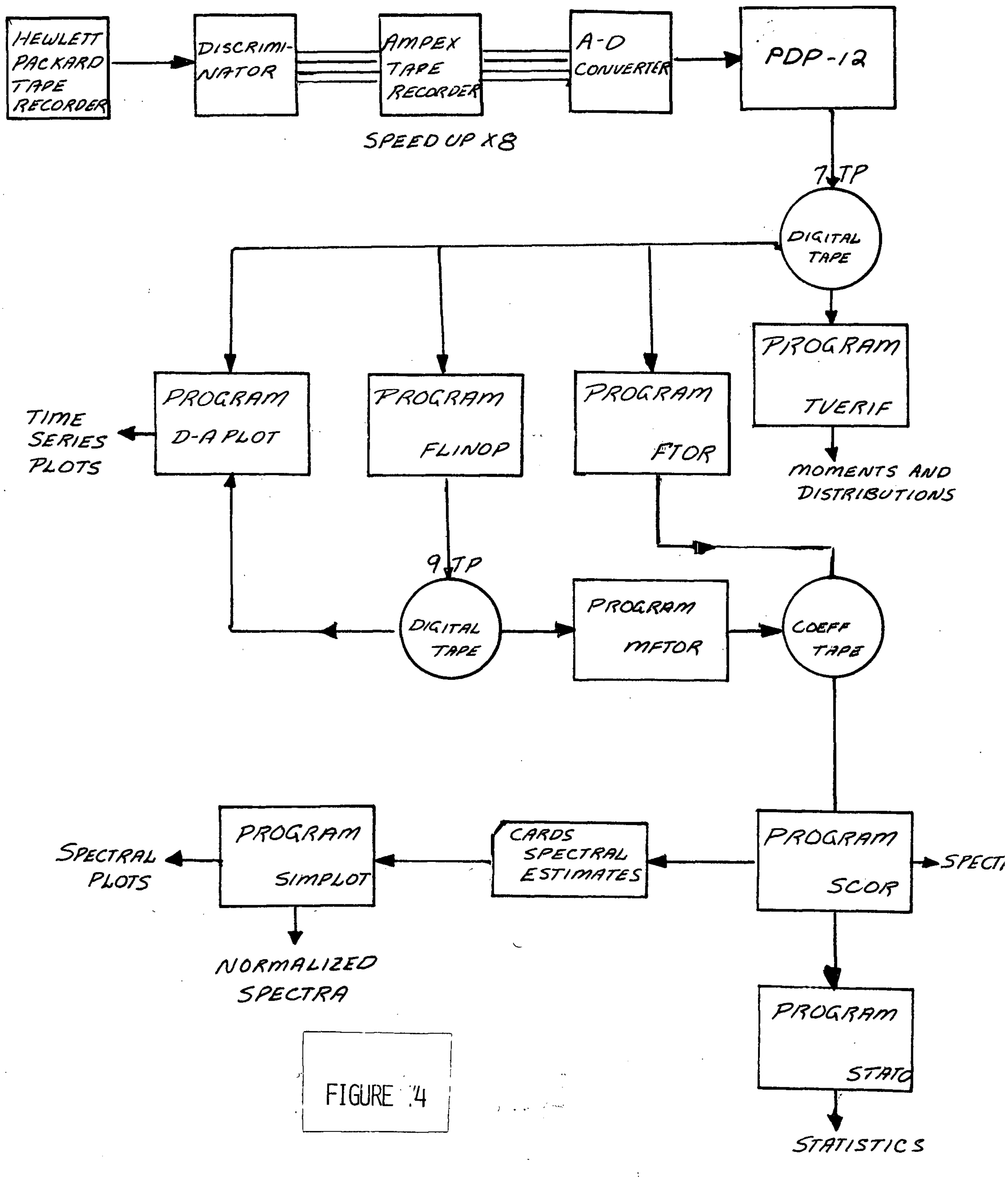
HEWLETT PACKARD TAPE RECORDER
DISCRIMI-NATOR
AMPEX TAPE RECORDER
A-D CONVERTER
PDP-12
SPEED UP X8
7 TP
DIGITAL TAPE
PROGRAM TVERIF
MOMENTS AND DISTRIBUTIONS
PROGRAM D-A PLOT
TIME SERIES PLOTS
PROGRAM FLINOP
PROGRAM FTOR
9 TP
DIGITAL TAPE
PROGRAM MFTOR
COEFF TAPE
PROGRAM SCOR
SPECT
CARDS SPECTRAL ESTIMATES
PROGRAM SIMPLOT
SPECTRAL PLOTS
NORMALIZED SPECTRA
PROGRAM STATO
STATISTICS

FIGURE 4

The data were digitized in 32 or 40 minute groupings at 75 hz. (real time). The PDP-12 wrote the sequentially sampled data on digital tape which made it compatible with the I.B.M. 360 system at U.B.C.

The program "TVERIF" acted as a check to see whether or not the digitization process was done properly. Voltage distributions for each channel and their first, second, third and fourth moments were displayed by the program. "FLINOP" was an operational program which allowed channels to be separately operated on. Such activities as adding, subtracting, multiplying, differentiating, box-car averaging and finding the square root of each channel could be done before making spectral estimates. The program "FTOR" used the fast Fourier transform method to convert each channel into Fourier coefficients. The coefficients were stored on tape and sent through the program "SCOR" which produced spectral and cross-spectral estimates. "SIMPLOT" accepted the spectral estimates from "SCOR" and gave the cumulative integral under the spectra as a function of decreasing frequency and also plotted the spectra and cospectra on a calcomp plotter.

CHAPTER 3

DISCUSSION OF RESULTS

3.1 Response Characteristics

The Sonic Anemometer and the Fluxatron measure wind components by different methods. Consequently, the response characteristics of each may not be the same and some comments are necessary before discussing the results.

3.1.1 General Comments on Propeller Response to Different Wind Speeds

Figure 5 shows the response of a four blade propeller to wind speeds from threshold to 5 ft/sec as given in the Gill Propeller Anemometer Manual. The response was zero within the threshold region and non-linear from threshold to about 3.5 ft/sec. Then after the response was 0.96 rev/ft. The non-linear region was the result of slippage and changing dynamic friction at low wind speeds. Frictional drag was responsible for the threshold region effects and a 0.96 rev/ft. response at high wind speeds.

Measurements of U' should not be affected by these response characteristics where $\overline{U}$ is large enough to keep the gill at speeds greater that 1.2 m/sec.

Figure 6 shows a proposed schematic response curve for the propeller where U_G is the gill wind speed and U is the true wind speed. The threshold and non-linear regions are marked and the dashed straight line represents a 1:1 slope.

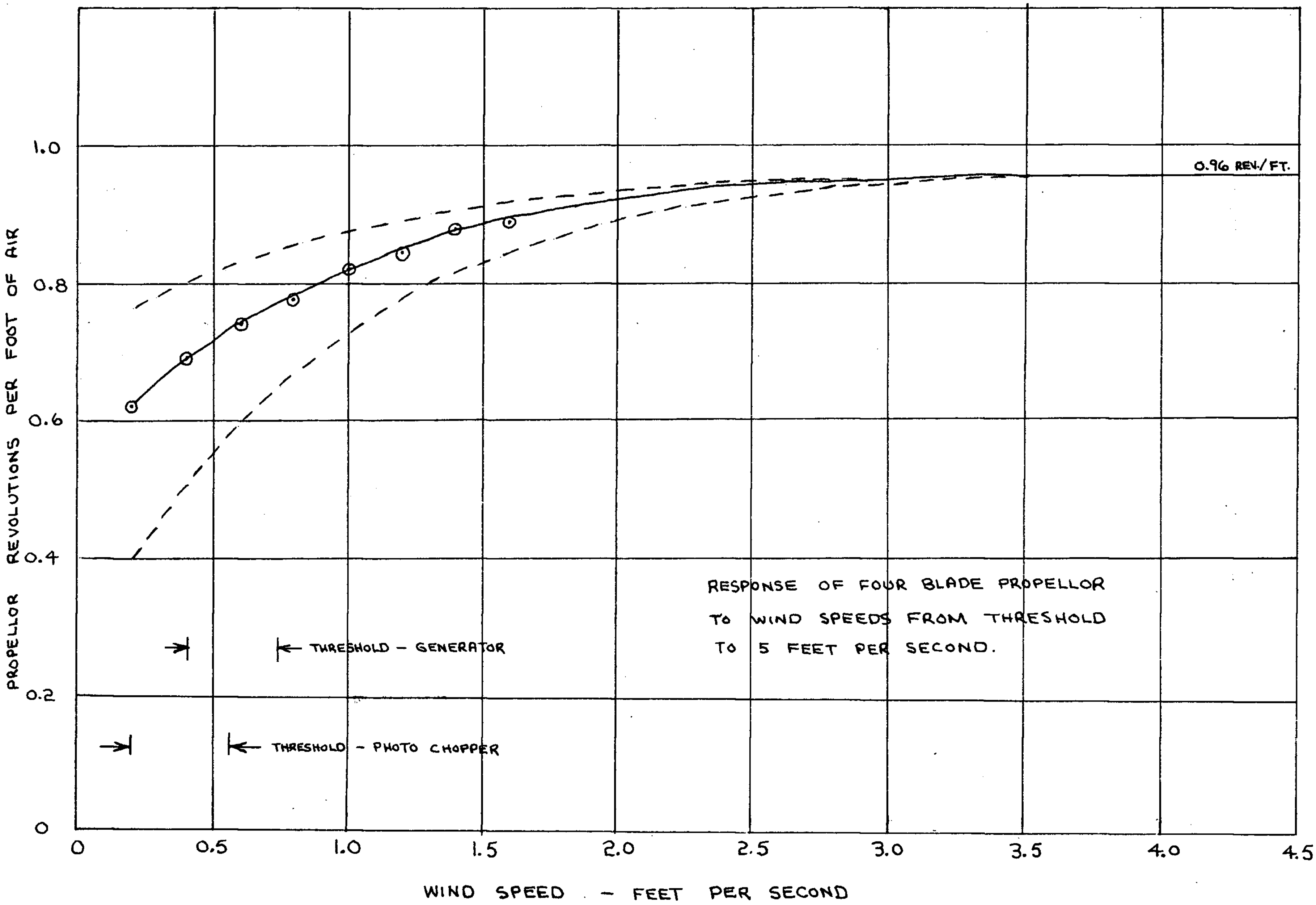
0.96 REV./FT.
1.0
0.8
0.6
0.4
0.2
0
PROPELLOR REVOLUTIONS PER FOOT OF AIR
RESPONSE OF FOUR BLADE PROPELLOR
TO WIND SPEEDS FROM THRESHOLD
TO 5 FEET PER SECOND.
THRESHOLD - GENERATOR
THRESHOLD - PHOTO CHOPPER
0
0.5
1.0
1.5
2.0
2.5
3.0
3.5
4.0
4.5
WIND SPEED - FEET PER SECOND

FIGURE 5

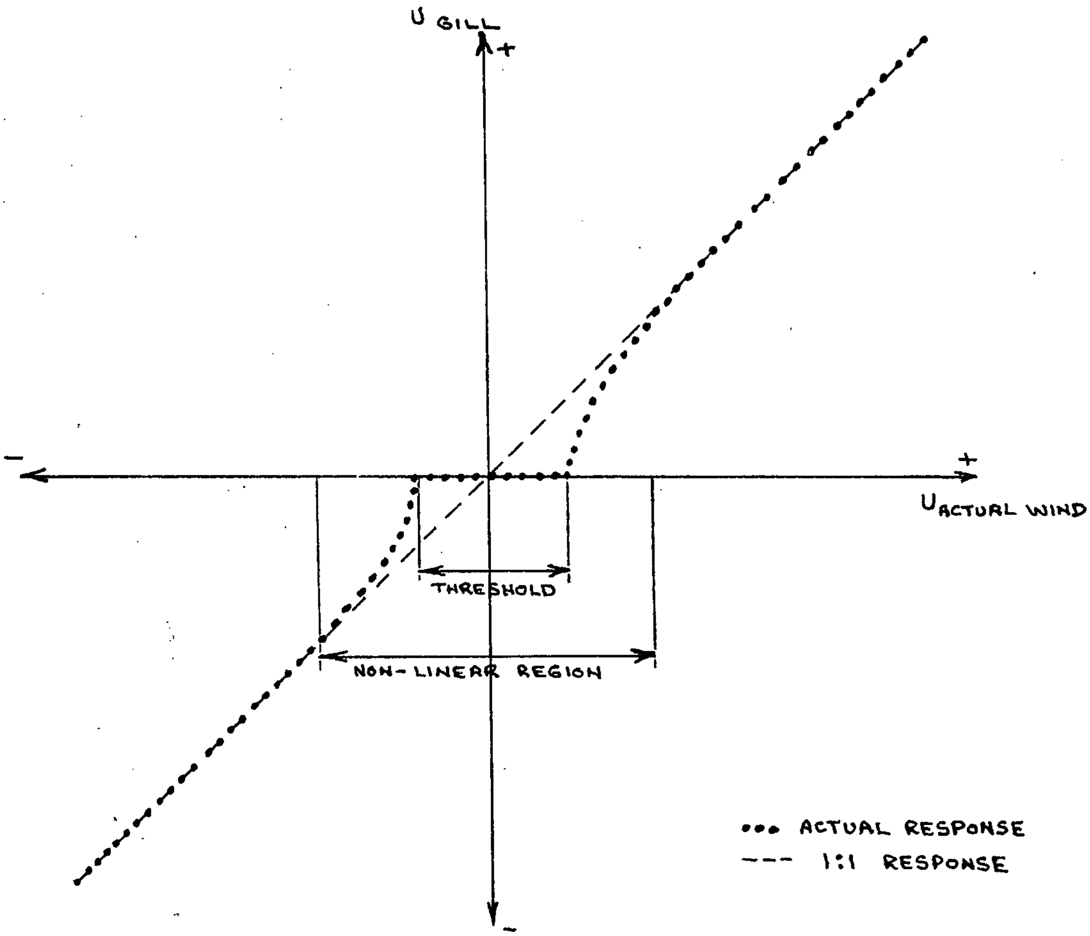

FIGURE #6. SCHEMATIC RESPONSE OF GILL ANEMOMETERS

One can approximate the curve by making U_{GILL} dependent on 1/U in the non-linear region:

$$U_G = U - b/U \tag{1}$$

where: U is actual wind and b is a constant.

Rewriting in quadratic form we have:

$$U^2 - U_G U - b = 0 \tag{2}$$

Or

$$U = U_G/2 \pm \sqrt{U_G^2 + 4b}/2 \tag{3}$$

To determine b we look at the threshold conditions:

$$U_G = 0 \text{ when } |U| \leq U_T$$

where: U_T is the threshold wind

Therefore from (2) we get:

$$b = U_T^2 - U_G U_T$$
$$\doteq U_T^2$$

Thus (3) becomes(for $|U| \geq U_T$):

$$U = 0.5\ (U_G \pm \sqrt{U_G^2 + 4U_T^2}\ ) \tag{4}$$

where under the square root sign the + sign is used when U > 0 and the - sign is used when U < 0.

As an example of the above formulation we can look at the case where $U_G = 0.50$ m/sec. and $U_T = 0.2$ m/sec.

The actual wind U is calculated by (4) to be 0.57 m/sec. Thus the amplitude of the Gill has dropped by 12%. When U_G first reaches zero the actual wind will still be 0.2 m/sec.

The frequency response of the Gill anemometer is expected to be more limited. In practice we can approximate its response by a low pass R-C filter in its output.

R-C filter theory defines the capacitive reactance as X_c, the resistance as R, the output potential as e_c, the input potential as e_s, and the phase shift as θ.

$$X_c = 1/2\pi fC \qquad e_c = e_s X_c / \sqrt{R^2 + X_c^2}$$

$$\theta = \arctan (R/X_c)$$

When the signal frequency is such that $X_c = R$ we define the cut off frequency f_c. The power dissipated across the resistor R is exactly half the apparent power, the output potential e_c is 0.707 e_s, and the phase shift is 45°.

When the Gill anemometer is used as a U' sensor the response characteristics are given in the terms of a distant constant X_L, where X_L is defined as the distance air must travel past the propeller before it turns at 0.707 the speed of the actual wind. The distance constant can be converted into a time constant by dividing by the mean wind ($t_L = X_L/\overline{U}$). This time constant is analogous to the R-C time constant discussed earlier.

Thus at the distance constant point the amplitude of the Gill output would be 0.707 the true amplitude, the phase shift between Gill and true would be 45° and the power spectrum attenuation would be 0.50.

3.1.2 Calibration Procedures

Sonic Anemometer

The sonic anemometer is an absolute instrument where fluctuations in sound speed are used to measure velocity fluctuations. A check of the calibration can be done in a wind tunnel. The calibration is maintained by periodic measurement of the time bases in analogue sections of the electronics. The response is linear for all wind speeds and its frequency response is good for frequencies up to 10 hz. where path length resolution becomes important.

Fluxatron

The fluxatron employs a Gill propeller anemometer with vane to measure U' and another propeller sensor to measure W'.

In order to calibrate a gill type anemometer the angular response of the sensor to the wind becomes very important. Figure 7 shows how the propeller responds to different wind angles. When the wind angle is zero (wind blowing directly into propeller) the response is 100%. However beyond 30° the actual response is below the ideal $\cos\theta$ response. Since normal wind flows do not exceed $\pm 30^{\circ}$ from the horizontal the effect would be minimal when the propeller is used for U' measurements. At $\pm 30^{\circ}$ the

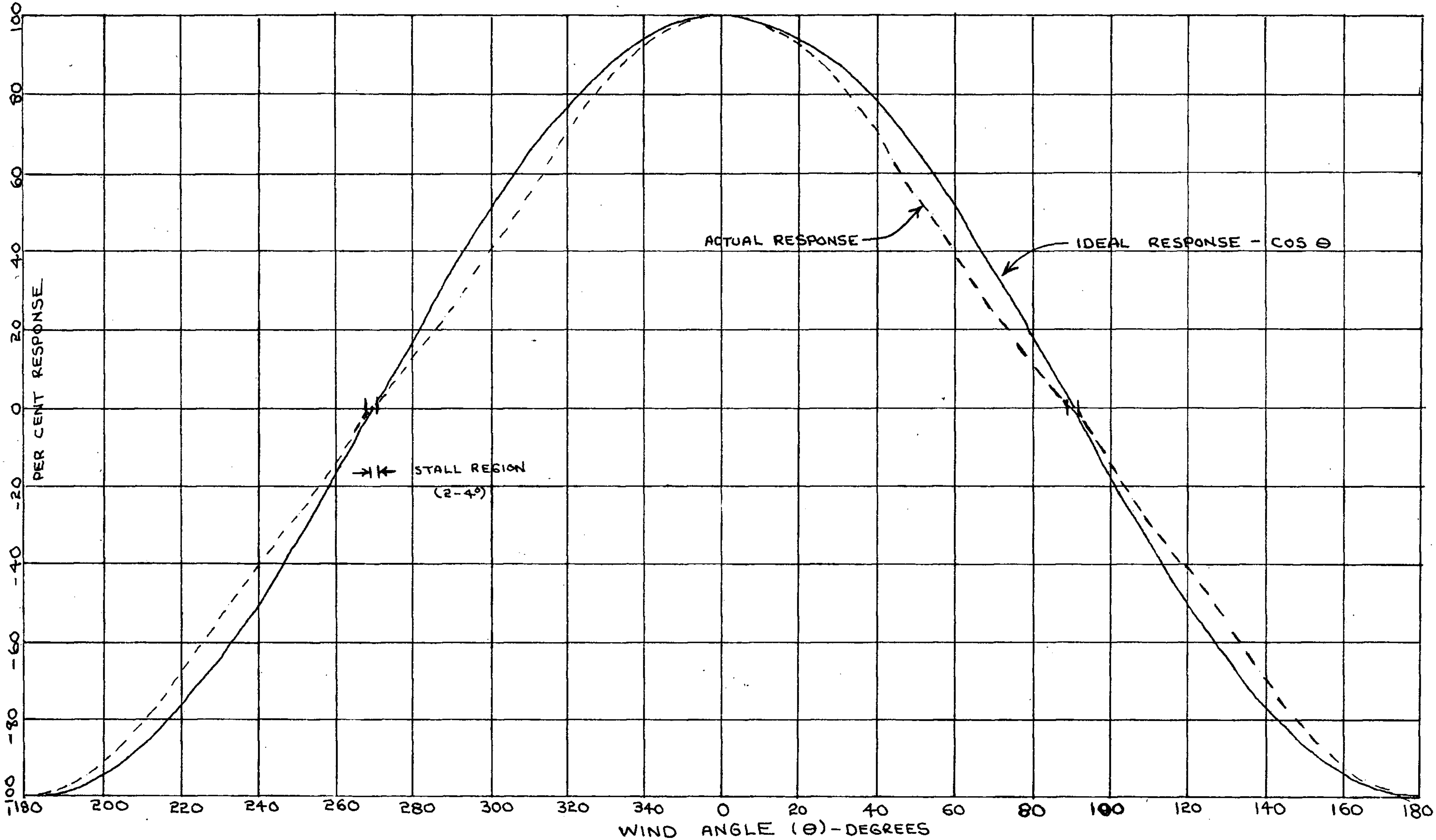

FIGURE 7 - PROPELLER RESPONSE VS WIND ANGLE (FROM GILL MANUAL)

response is down an extra 6%

The actual calibration of each U' gill can be done in the wind tunnel. This allows the estimation of the threshold region, the non-linear region, and the linear region. The calibration is good for the total component of the horizontal wind.

For the vertical gill calibration the cosine response of the propeller is needed since in operation the vertical sensor is consistently measuring components of the wind.

In practice the sonic W' signal and the Fluxatron W' should agree for large amplitude low frequency fluctuations if both are calibrated properly. This particular procedure was used in this study to check the calibration of the signals from the Tsimlyansk field data.

3.2 Discussion of Data

3.2.1 Measurements of Horizontal Velocity

The time traces of U' from the Fluxatron should be void of non-linear effects when mean winds are in excess of about 3 m/sec. To check this the linear sonic U' trace was compared to the Fluxatron output. Figure 8 shows time domain traces of U' for Run T029. Actual outputs are shown from both instruments and also three filtered traces of the sonic U'. A Krohnhite Filter (model 3340) with a sharp low-pass filtering characteristic was used. The filtered output was specified to be down 18.5 db. at cut-off and to have a 48 db. per octave attenuation slope. The basic

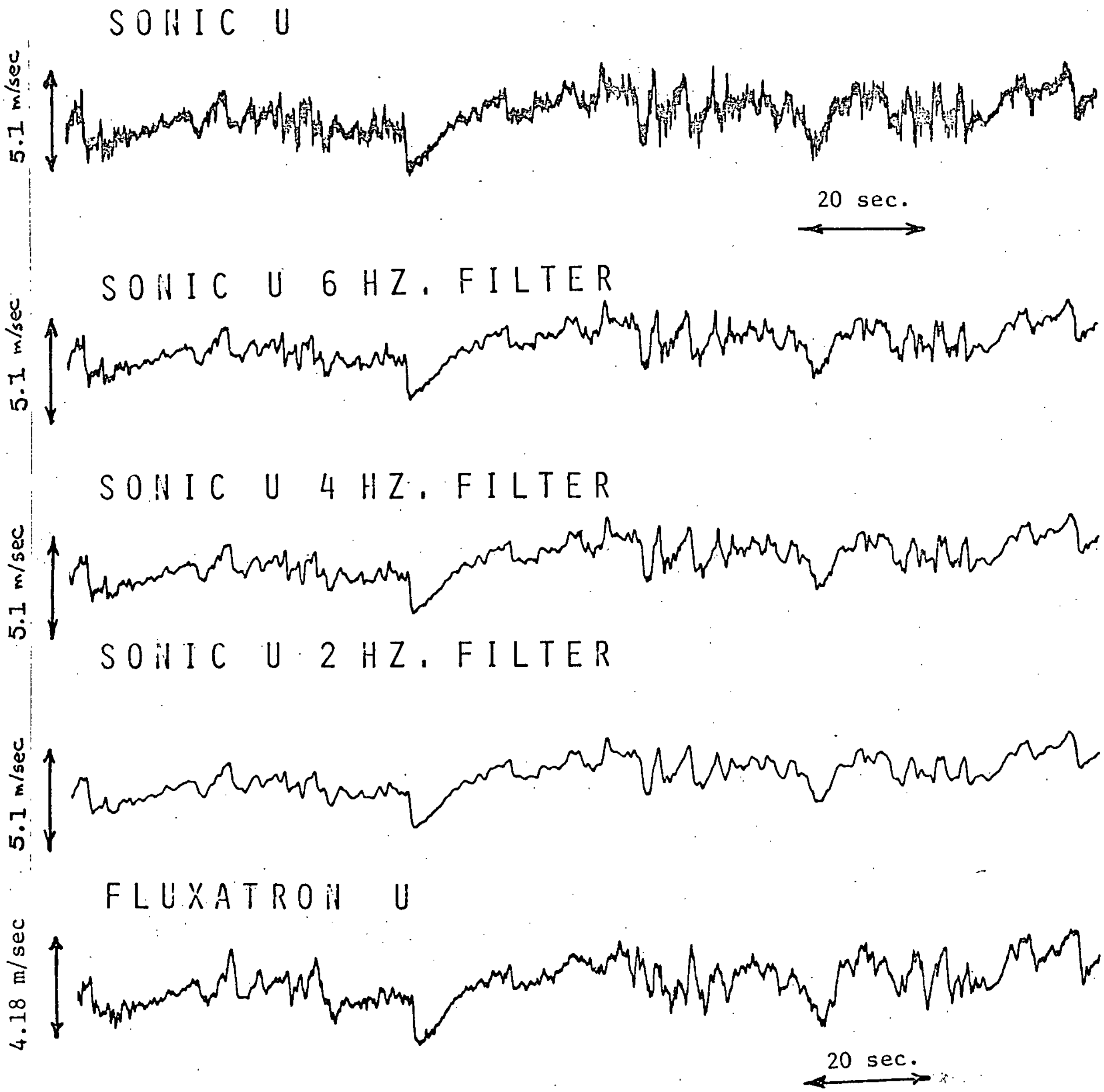

FIGURE 8 - TIME TRACES OF U'

agreement in shape and magnitude of the sonic and propeller was good as shown in Figure 8. Best visual shape agreement was observed when frequencies greater than about 6 hz. had been removed by the Krohnhite from the Sonic U' signal.

The cut-off frequency f_c at half power turns out to be at 1.4 hz. for a Krohnhite setting of 6 hz. (checked by filtering the sonic spectra separately). The distant constant for this case would then be of the order $\frac{\overline{U}}{f_c} = \frac{5.8}{1.4} = 4.1$ m.

Figures 9, 10 and 11 show spectral computations for three runs. Plots designated with a 1 represent U.B.C. sonic measurements, those with a 2 Russian Sonic Measurements, and those with a 3 the Fluxatron Measurements. In the region below about f = 2×10^{-1} hz. the spectra agreed closely in shape and magnitude. For frequencies greater than 2×10^{-1} hz., the high frequency attenuation of the gill began to affect the results. The Fluxatron spectra was attenuated by a factor of ½ at about 1 hz. Table 2 shows estimate of $\overline{U'^2}$ cumulative integrals for these regions. The average ratio of the total variances for the Fluxatron/sonic was 1.08. The Fluxatron in general appeared to overestimate the wind slightly, a possible calibration problem.

Figures 12, 13 and 14 show ratios of the spectral amplitudes plotted against frequency for the three runs. The agreement below f = 2×10^{-1} was approximately 1.2:1 except at very low frequencies where high pass filters in the Fluxatron electronics became significant. Above

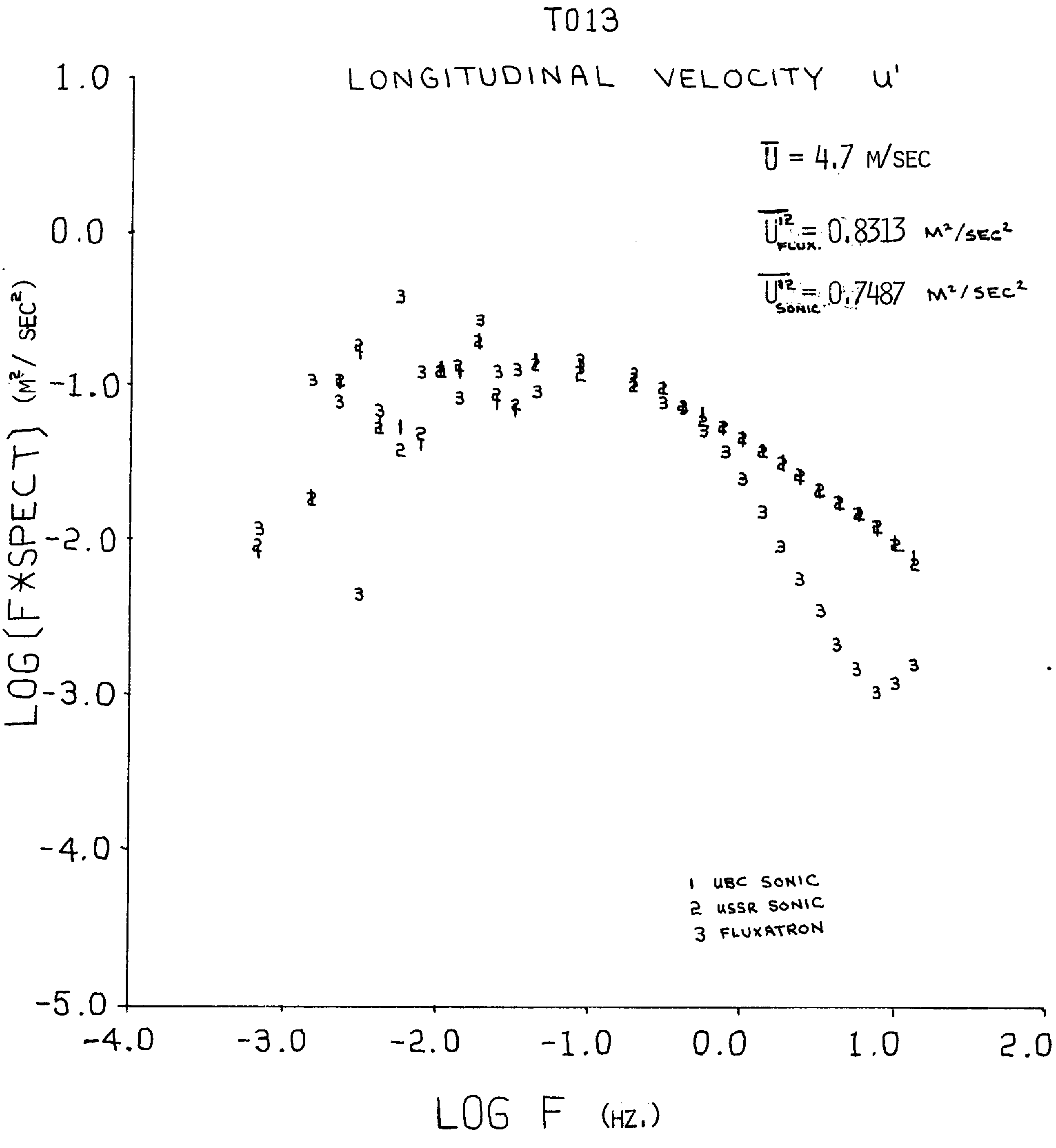

T013
LONGITUDINAL VELOCITY u'
$\overline{U}$ = 4.7 M/SEC
$\overline{U'^2}_{FLUX.}$ = 0.8313 M²/SEC²
$\overline{U'^2}_{SONIC}$ = 0.7487 M²/SEC²
1 UBC SONIC
2 USSR SONIC
3 FLUXATRON
LOG(F*SPECT) (M²/SEC²)
LOG F (HZ.)
1.0
0.0
-1.0
-2.0
-3.0
-4.0
-5.0
-4.0
-3.0
-2.0
-1.0
0.0
1.0
2.0

FIGURE 9

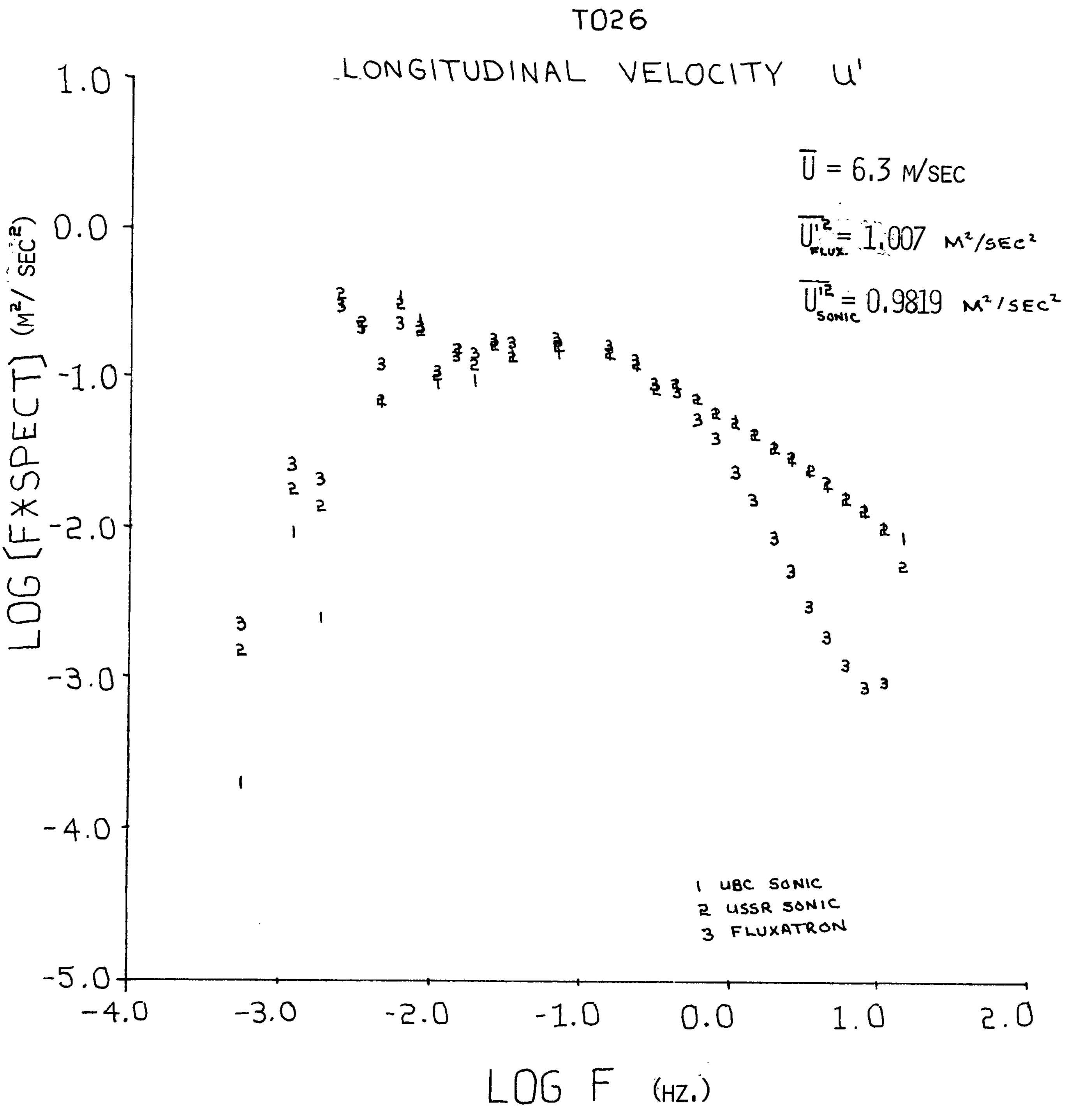
T026
LONGITUDINAL VELOCITY U'
$\overline{U}$ = 6.3 M/SEC
$\overline{U'^2_{FLUX}}$ = 1.007 M²/SEC²
$\overline{U'^2_{SONIC}}$ = 0.9819 M²/SEC²
1 UBC SONIC
2 USSR SONIC
3 FLUXATRON
LOG [F*SPECT] (M²/SEC²)
LOG F (HZ.)
1.0
0.0
-1.0
-2.0
-3.0
-4.0
-5.0
-4.0
-3.0
-2.0
-1.0
0.0
1.0
2.0

FIGURE 10

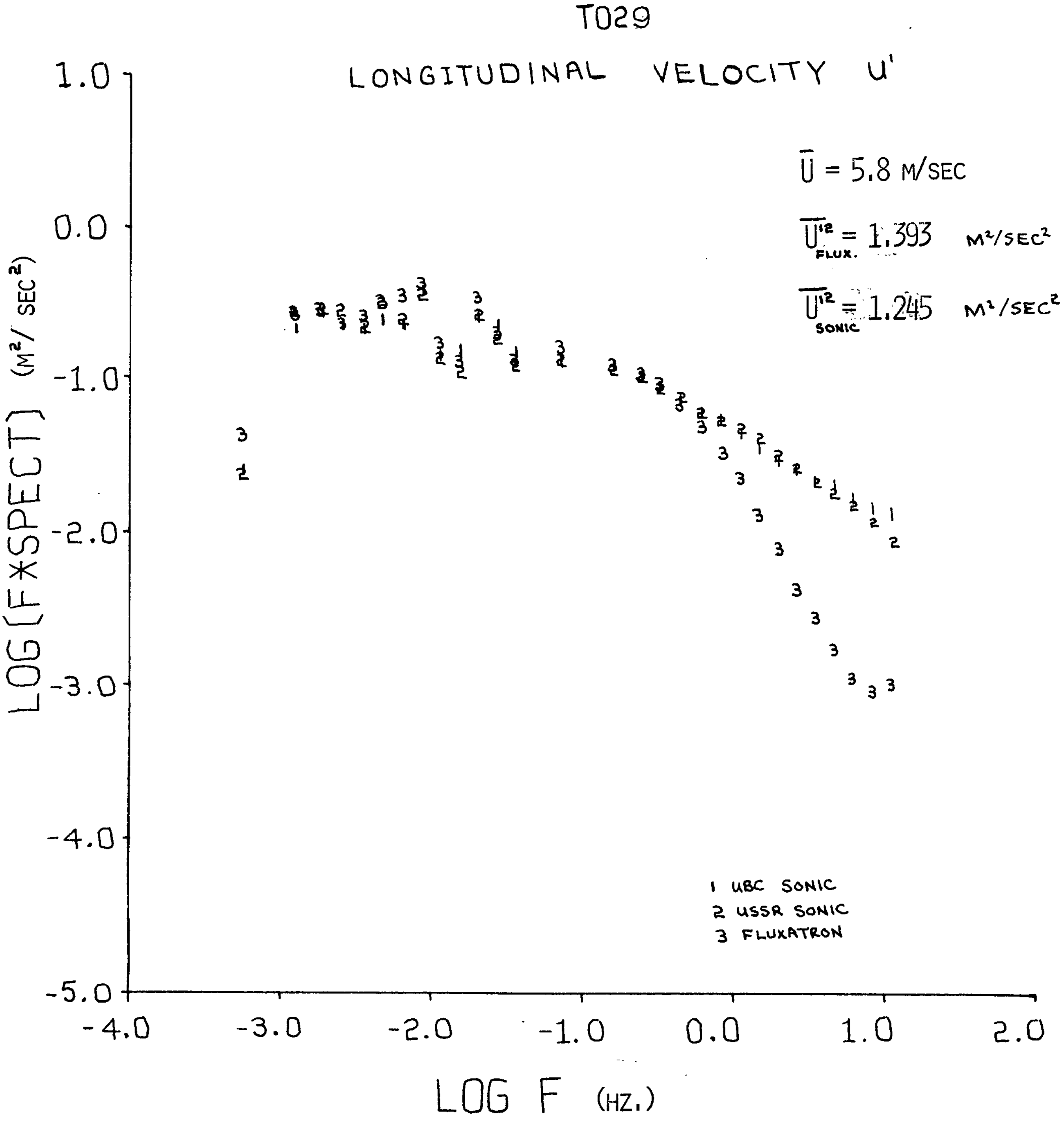
T029
LONGITUDINAL VELOCITY U'
$\overline{U}$ = 5.8 M/SEC
$\overline{U'^2}_{FLUX.}$ = 1.393 M²/SEC²
$\overline{U'^2}_{SONIC}$ = 1.245 M²/SEC²
LOG(F*SPECT) (M²/SEC²)
1.0
0.0
-1.0
-2.0
-3.0
-4.0
-5.0
-4.0
-3.0
-2.0
-1.0
0.0
1.0
2.0
LOG F (HZ.)
1 UBC SONIC
2 USSR SONIC
3 FLUXATRON

FIGURE 11

TABLE 2

U'U' CUMULATIVE INTEGRALS

(M.K.S. UNITS)

.00055hz.<f<.158hz.

RUN	FLUXATRON	SONIC(UBC)	SONIC(USSR)	FLUX./SONIC(UBC)
T013	0.6744	0.5192	0.5077	1.29
T026	0.7820	0.7086	0.7350	1.10
T029	1.205	1.005	1.066	1.20

.158hz.<f< 10.8hz.

RUN	FLUXATRON	SONIC(UBC)	SONIC(USSR)	FLUX./SONIC(UBC)
T013	0.1569	0.2095	0.2026	0.749
T026	0.2250	0.2733	0.2750	0.823
T029	0.1880	0.2400	0.2360	0.783

.00055hz.<f< 10.8hz.

RUN	FLUXATRON	SONIC(UBC)	SONIC(USSR)	FLUX./SONIC(UBC)
T013	0.8313	0.7487	0.7103	1.11
T026	1.007	0.9819	1.010	1.02
T029	1.393	1.245	1.302	1.12

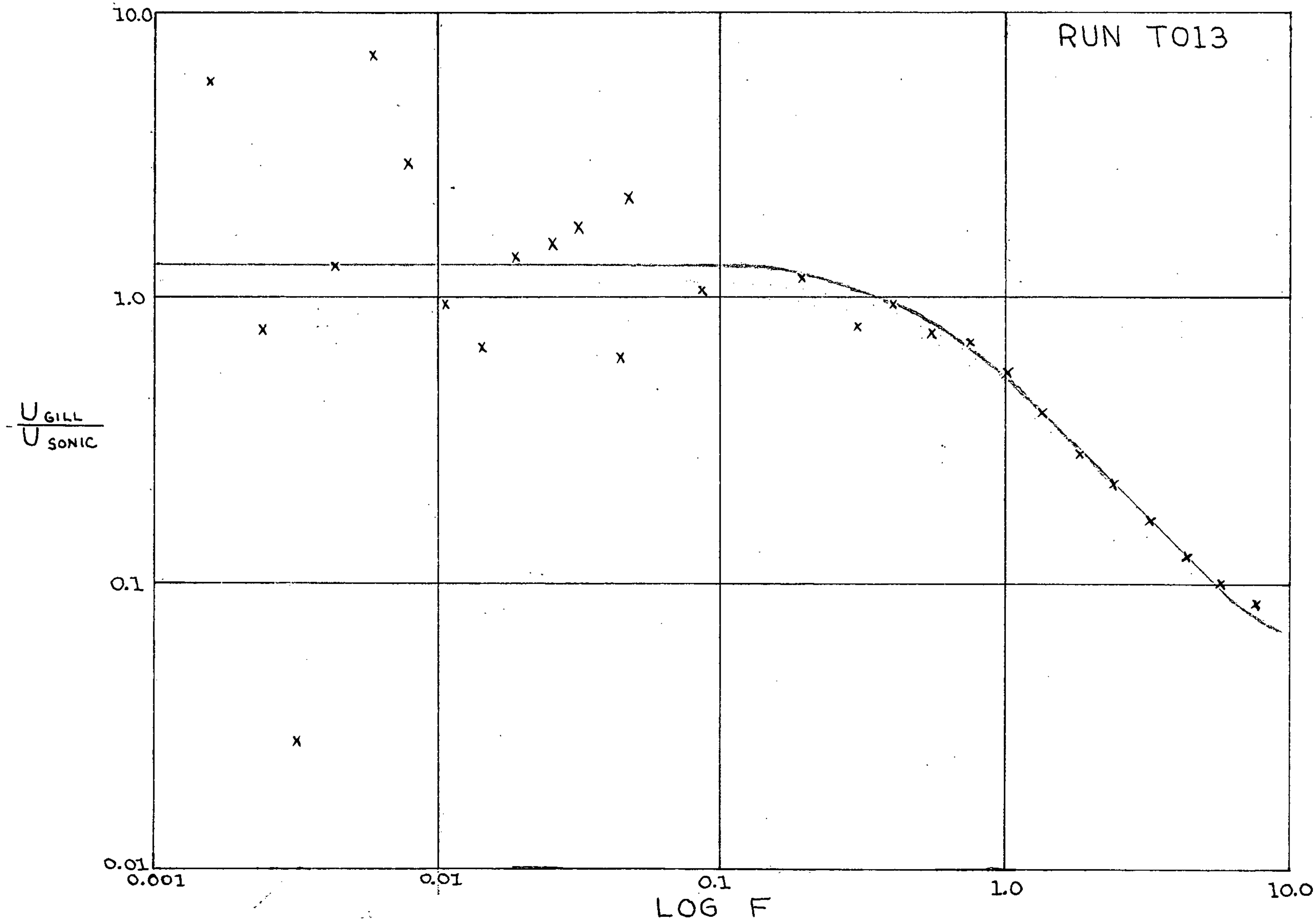

FIGURE 12 - RATIO OF SPECTRAL ESTIMATES

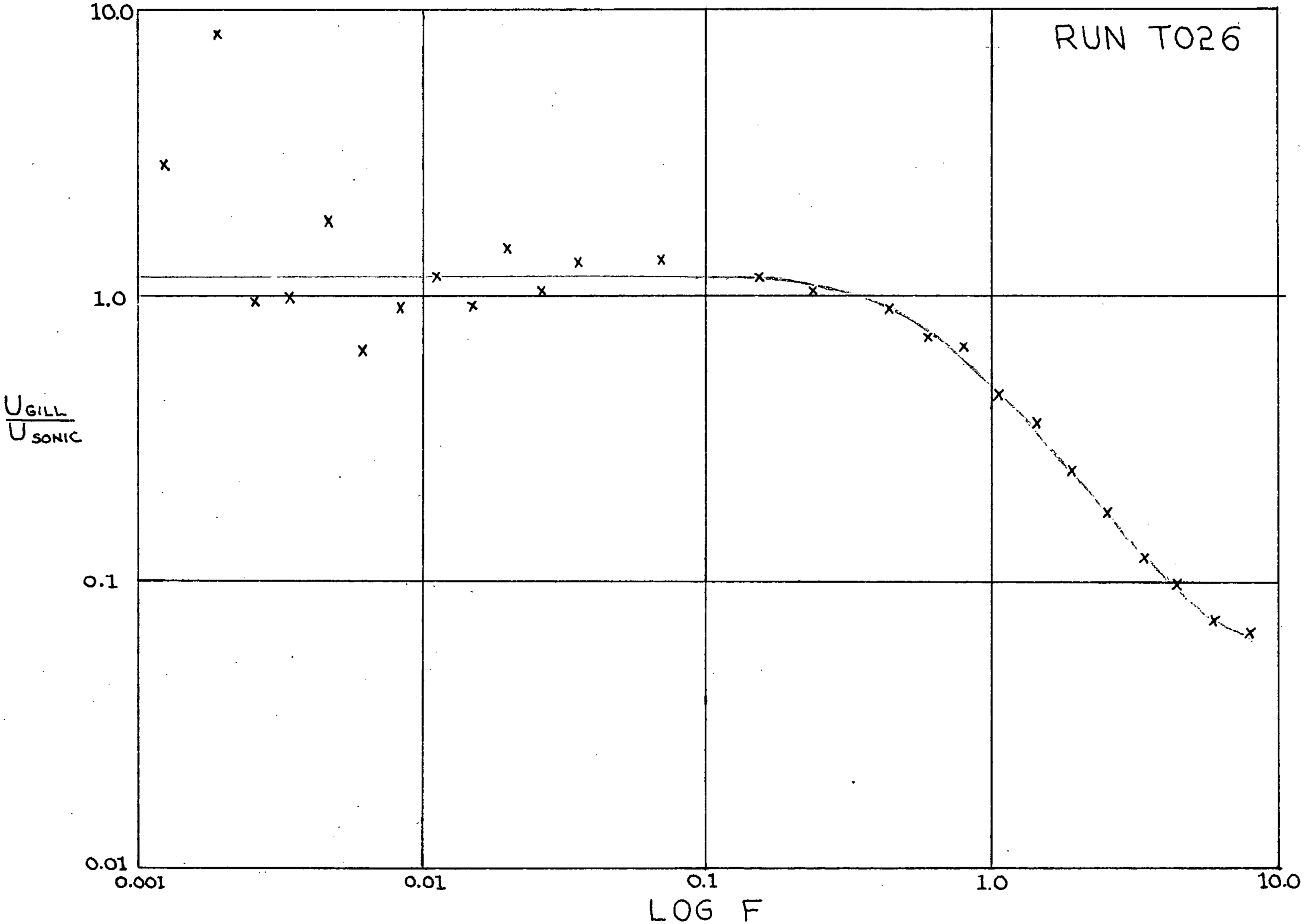

FIGURE 13 – RATIO OF SPECTRAL ESTIMATES

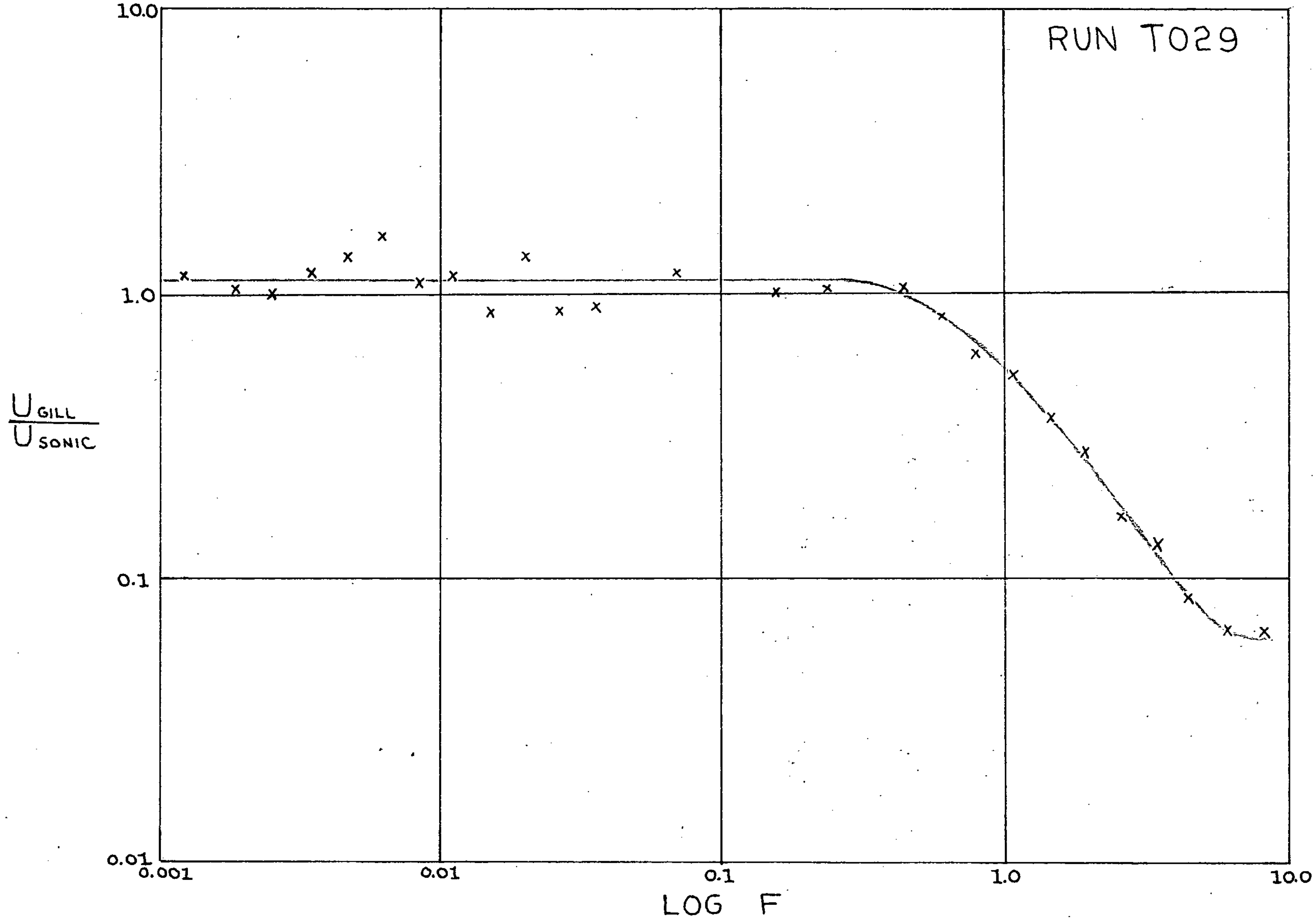

FIGURE 14 – RATIO OF SPECTRAL ESTIMATES

$f = 2 \times 10^{-1}$ hz. the ratio began to drop. The Fluxatron power was reduced to ½ at f = 0.70 hz., f = 0.85 hz, and f = 0.90 hz. for Runs T013, T026, T029 respectively. The mean winds from profile measurements were 4.7 m/sec, 6.3 m/sec, and 5.8 m/sec respectively. Thus, the associated distant constants would be 6.72 m., 7.54 m., and 6.47., (from $X_L = \bar{U} / 2\pi f$) for Runs T013, T026, and T029 respectively.

Figure 15 shows the joint probability density of U' sonic across and U' propeller down. The contours represent lines of constant density at intervals of 200. The ridge of highest density marked with a dotted line represents a best approximation of the actual response of the two instruments. The response was 1:1 and linear between outputs of ± 1.0 and then showed a slight tendency for higher sonic values at larger outputs. This characteristic of the signal's was probably a result of the high frequency limitations of the Gill. Peak values of the higher frequency Sonic Fluctuations should be greater than the Gill beyond cut-off.

Figure 16 shows the probability distribution of both U' signals. The skewed nature of the velocity distribution was noted. Both the sonic and Gill propeller showed peak distribution in the same region with the Sonic showing a higher probability. The horizontal axis is such that higher velocities were to the right (in the positive region)

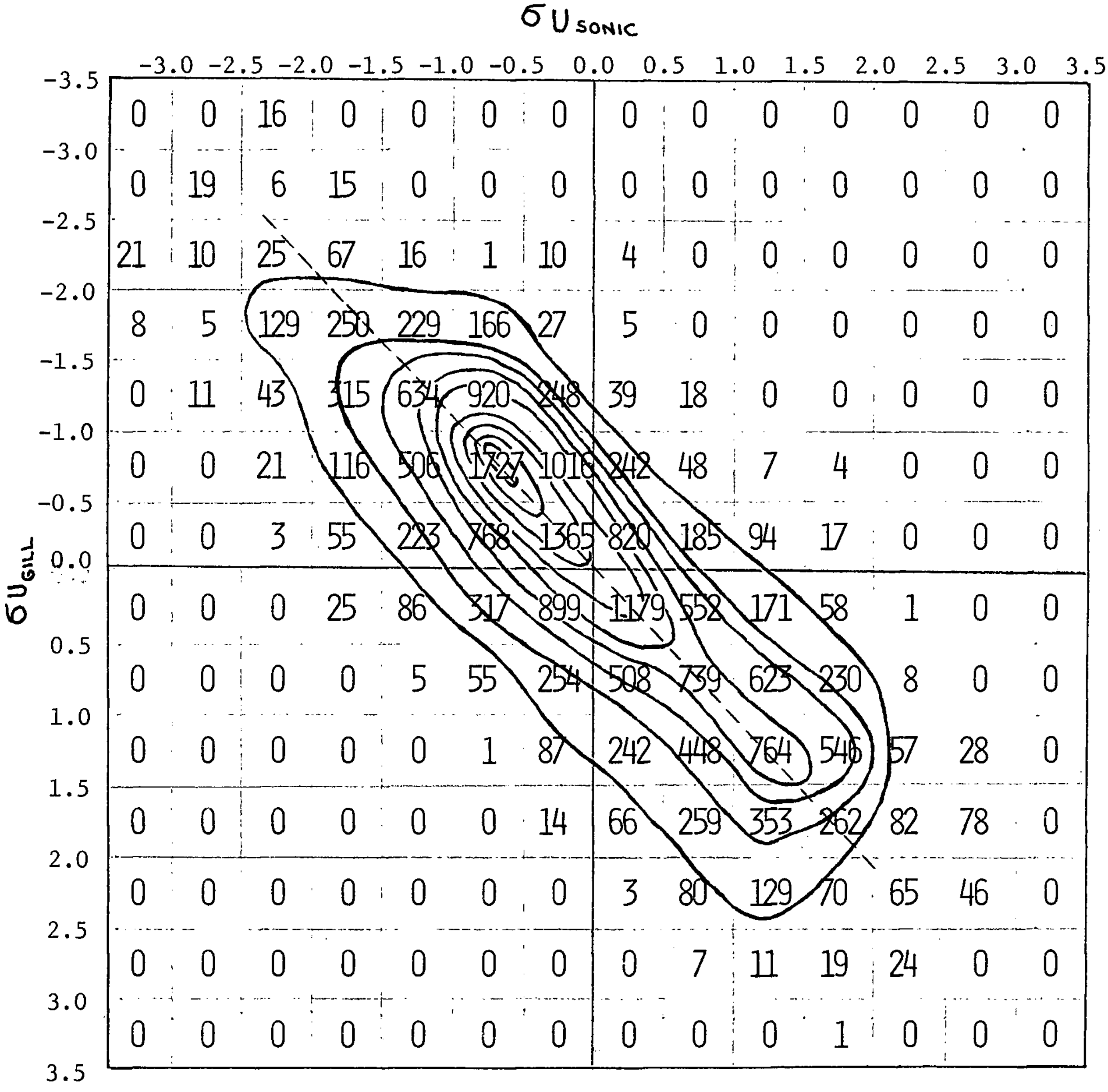

σU GILL \ σU SONIC	-3.5 to -3.0	-3.0 to -2.5	-2.5 to -2.0	-2.0 to -1.5	-1.5 to -1.0	-1.0 to -0.5	-0.5 to 0.0	0.0 to 0.5	0.5 to 1.0	1.0 to 1.5	1.5 to 2.0	2.0 to 2.5	2.5 to 3.0	3.0 to 3.5
-3.5 to -3.0	0	0	16	0	0	0	0	0	0	0	0	0	0	0
-3.0 to -2.5	0	19	6	15	0	0	0	0	0	0	0	0	0	0
-2.5 to -2.0	21	10	25	67	16	1	10	4	0	0	0	0	0	0
-2.0 to -1.5	8	5	129	250	229	166	27	5	0	0	0	0	0	0
-1.5 to -1.0	0	11	43	315	634	920	248	39	18	0	0	0	0	0
-1.0 to -0.5	0	0	21	116	506	1727	1016	242	48	7	4	0	0	0
-0.5 to 0.0	0	0	3	55	223	768	1365	820	185	94	17	0	0	0
0.0 to 0.5	0	0	0	25	86	317	899	1179	552	171	58	1	0	0
0.5 to 1.0	0	0	0	0	5	55	254	508	739	623	230	8	0	0
1.0 to 1.5	0	0	0	0	0	1	87	242	448	764	546	57	28	0
1.5 to 2.0	0	0	0	0	0	0	14	66	259	353	262	82	78	0
2.0 to 2.5	0	0	0	0	0	0	0	3	80	129	70	65	46	0
2.5 to 3.0	0	0	0	0	0	0	0	0	7	11	19	24	0	0
3.0 to 3.5	0	0	0	0	0	0	0	0	0	0	1	0	0	0

NORMALIZED

FIGURE 15 - JOINT PROBABILITY DENSITY OF U GILL AND U SONIC

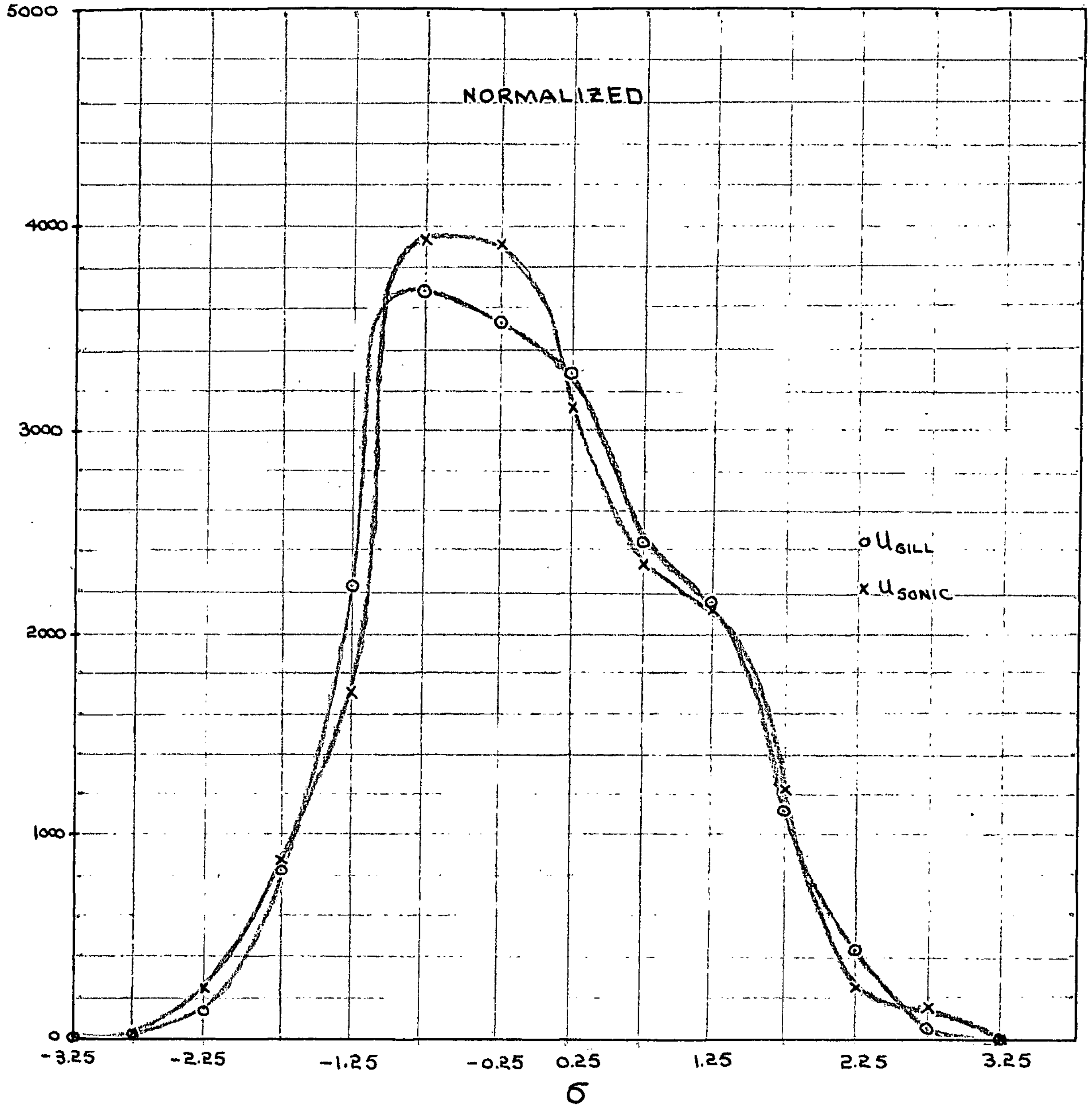

FIGURE 16 - PROBABILITY DISTRIBUTION OF U GILL AND U SONIC

and lower velocities to the left (negative region). Both sonic and Gill observed a second peak in distribution in the positive or higher wind speed area of the velocity field.

Figure 17 shows a plot of the coherence and phase for the Fluxatron U' and sonic U' (U.S.S.R.) signals of Run T029. One defines coherence as:

$$\text{Coherence:} \quad \text{coh}_{xy}(n) = \left(\frac{S^2{}_{xy}(n) + Q^2{}_{xy}(n)}{S_{xx}(n) \times S_{yy}(n)} \right)^{\frac{1}{2}}$$

where S_{xy} and $Q_{xy}(n)$ are the cospectrum and quadspectrum respectively. The coherence was near 1 at f = 0.01 hz. and had fallen off to 0.5 at f = 0.9 hz. The phase lag of the propeller was near zero at the lowest frequencies and reached 45° by about f = 0.75 hz. If we assume this was the point of frequency cut-off according to theory, this corresponded to a distance constant of $\frac{\bar{U}}{2\pi f} = \frac{5.8}{6.28(0.75).75} = 7.91$ m. which compared with the result attained by looking at the ratios of power spectra (6.91 metres) respectively.

3.2.2 Measurements of Vertical Velocity

Figure 18 shows time domain traces of W' signals. Actual voltage outputs are shown from the Fluxatron and the U.B.C. Sonic and also three filtered traces of the Sonic W'. The visual agreement in both shape and magnitude is less than it was for the U' traces.

Spacing of the sensors can sometimes introduce sampling problems. However, the cross-stream separation for these runs was always in the order of 1 metre so that larger scale

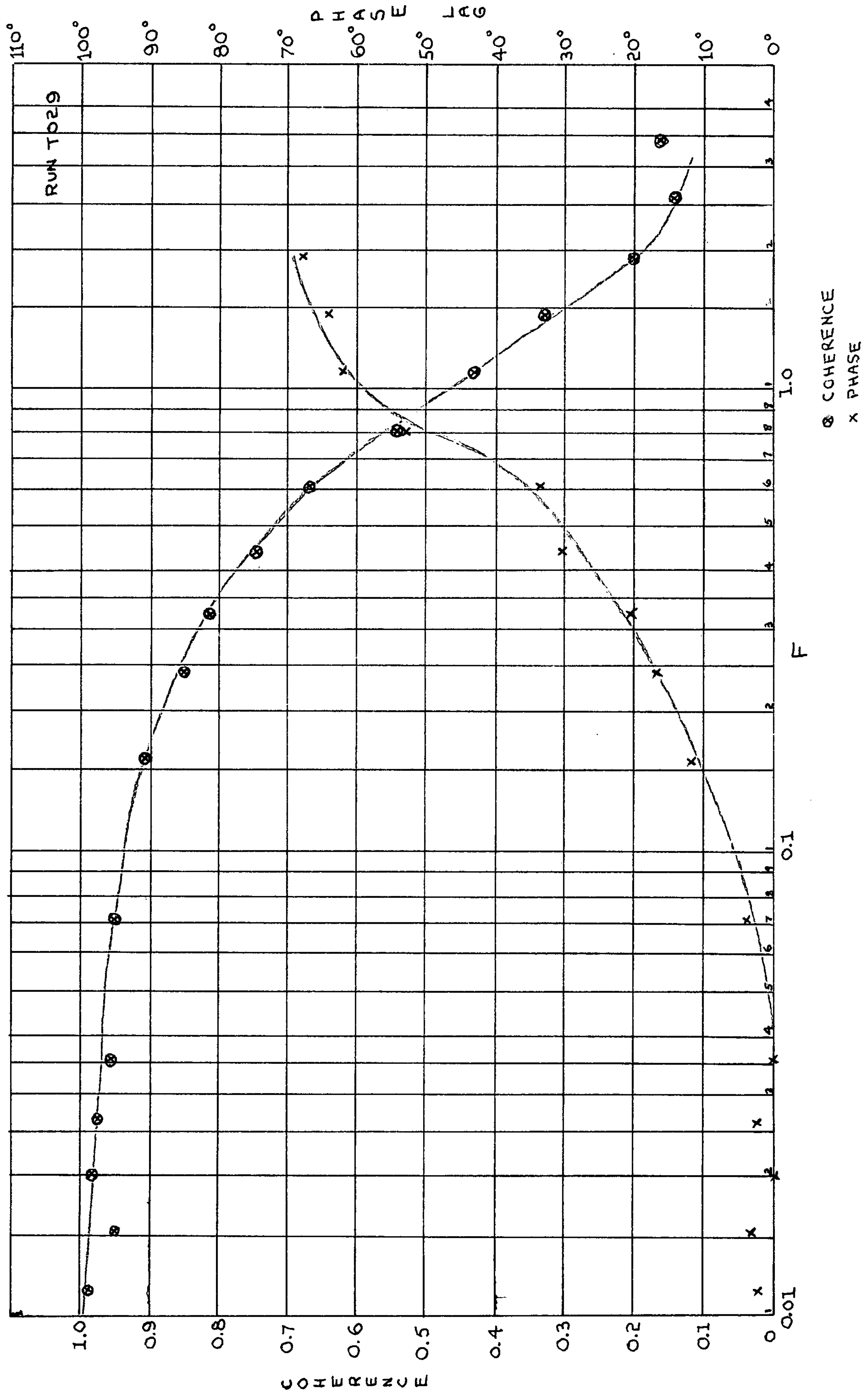
RUN T029
PHASE LAG
110° 100° 90° 80° 70° 60° 50° 40° 30° 20° 10° 0°
COHERENCE
1.0 0.9 0.8 0.7 0.6 0.5 0.4 0.3 0.2 0.1 0
F
0.01 0.1 1.0
⊗ COHERENCE
x PHASE

FIGURE 17

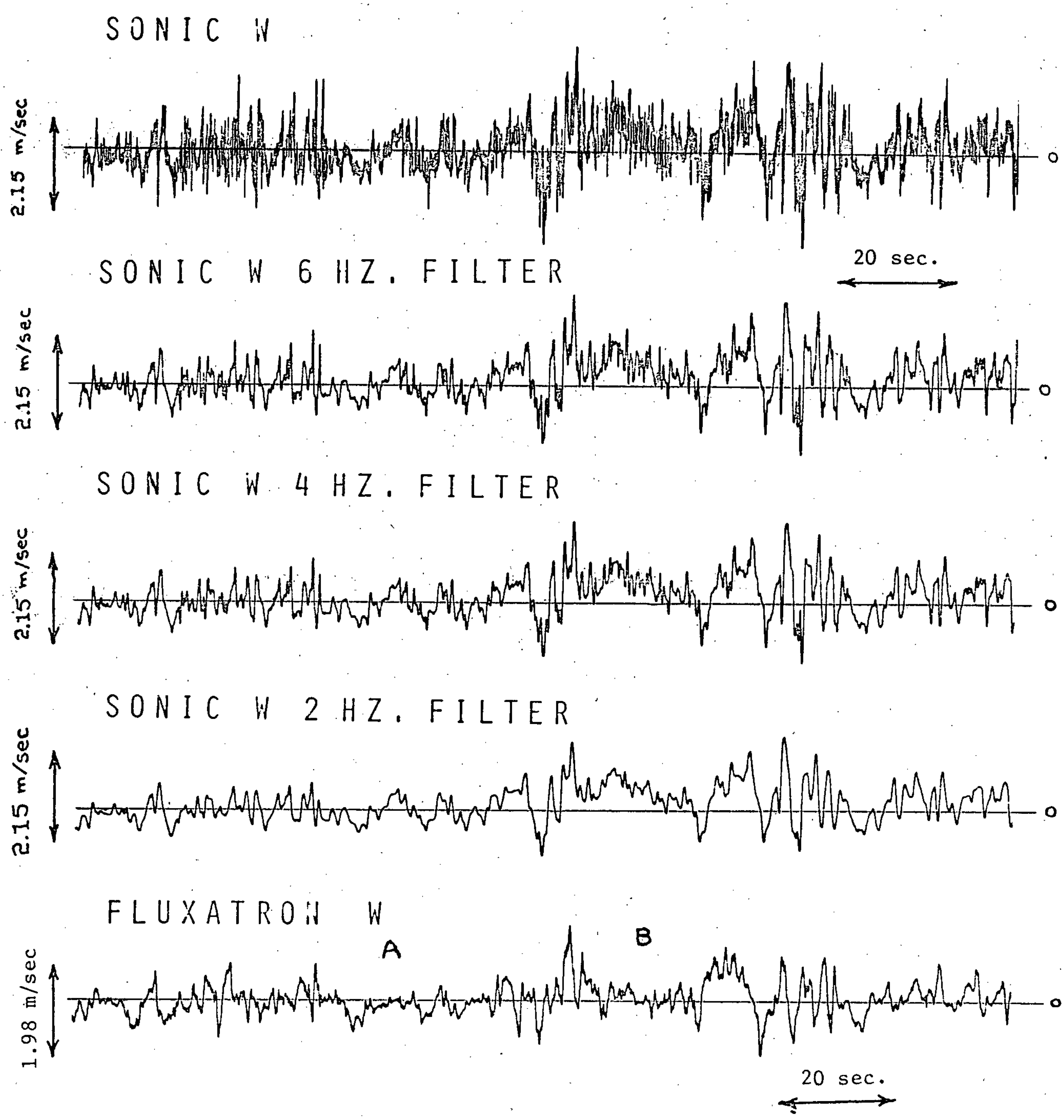
SONIC W
2.15 m/sec
0
SONIC W 6 HZ. FILTER
20 sec.
2.15 m/sec
0
SONIC W 4 HZ. FILTER
2.15 m/sec
0
SONIC W 2 HZ. FILTER
2.15 m/sec
0
FLUXATRON W
A
B
1.98 m/sec
0
20 sec.

FIGURE 18

vertical gusts should still have agreed if the instrument responses were similar. Comparison with the two acoustic anemometers indicated this to be the case.

Figure 18 showed that in general the best agreement in shape was attained using 2-4hz. Krohnhite filters on Sonic W'. Comparing it with the propeller W', it was observed that near where W' = 0, there was little fluctuating energy from the propeller but still considerable energy associated with sonic W'. Areas A and B on the traces emphasize this statement. Part A indicates a loss in amplitude of higher frequency fluctuations in the propeller signal as cf. to the sonic. Part B shows a loss in amplitude of both higher and lower frequency fluctuations associated with the propeller. In Part B, a definite low frequency trend in sonic W' was not seen at all by the propeller. As pointed out by the scale of the traces a large percentage of the time was spent operating in the non-linear range ($\pm$ 1.00 m/sec.).

This particular loss of W' information from the propeller had a direct effect on the computation of the momentum flux as will be shown later in a discussion of the cospectra of U' and W'.

In order to look at the energy contributions at all frequency levels for both sonic and Fluxatron W' signals, Figures 19, 20 and 21 were shown. Each W' signal was displayed at different filtering stages down to 0.3 hz. low

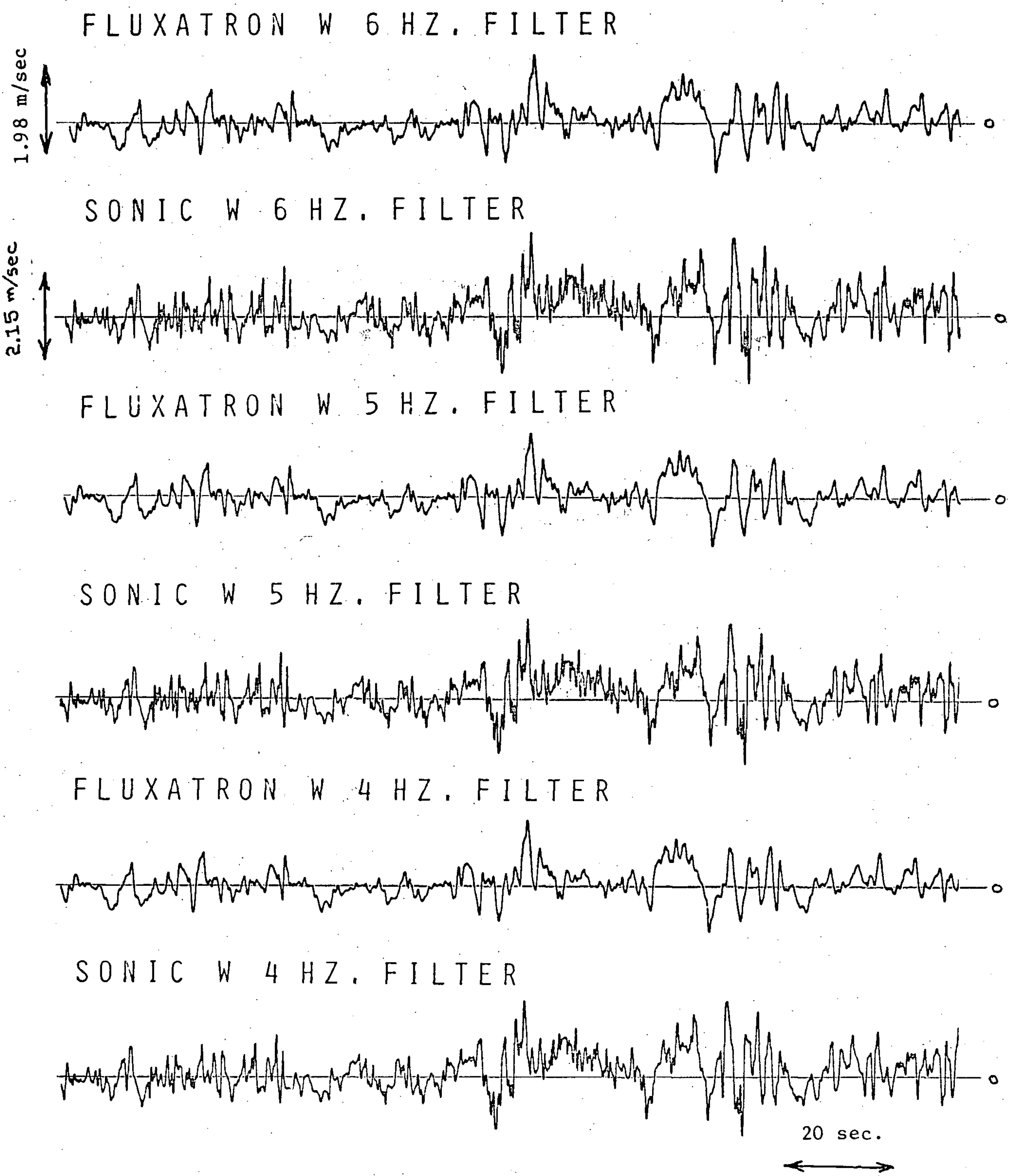
FLUXATRON W 6 HZ. FILTER
1.98 m/sec
0
SONIC W 6 HZ. FILTER
2.15 m/sec
0
FLUXATRON W 5 HZ. FILTER
0
SONIC W 5 HZ. FILTER
0
FLUXATRON W 4 HZ. FILTER
0
SONIC W 4 HZ. FILTER
0
20 sec.

FIGURE 19

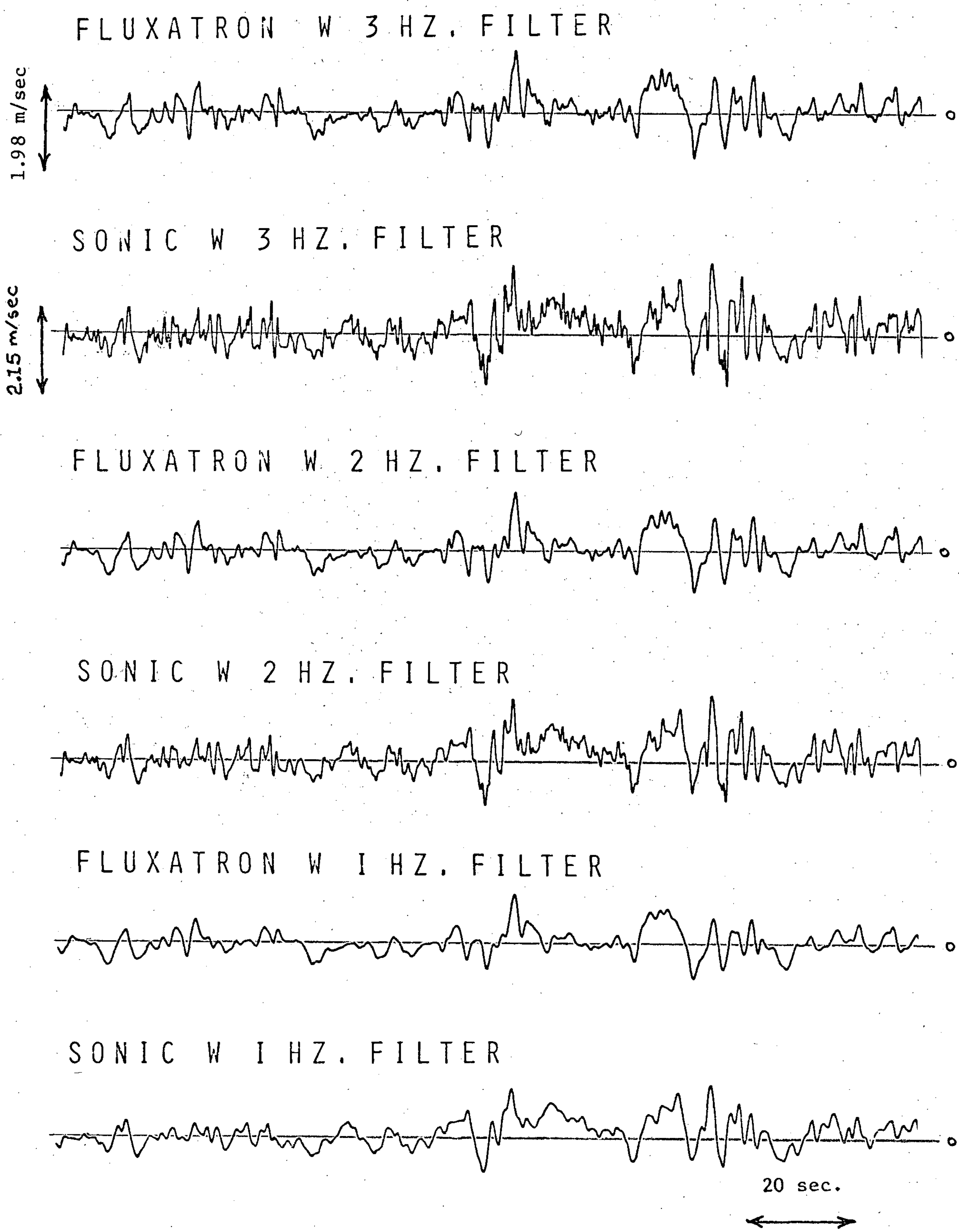
FLUXATRON W 3 HZ. FILTER
1.98 m/sec
0
SONIC W 3 HZ. FILTER
2.15 m/sec
0
FLUXATRON W 2 HZ. FILTER
0
SONIC W 2 HZ. FILTER
0
FLUXATRON W I HZ. FILTER
0
SONIC W I HZ. FILTER
0
20 sec.

FIGURE 20

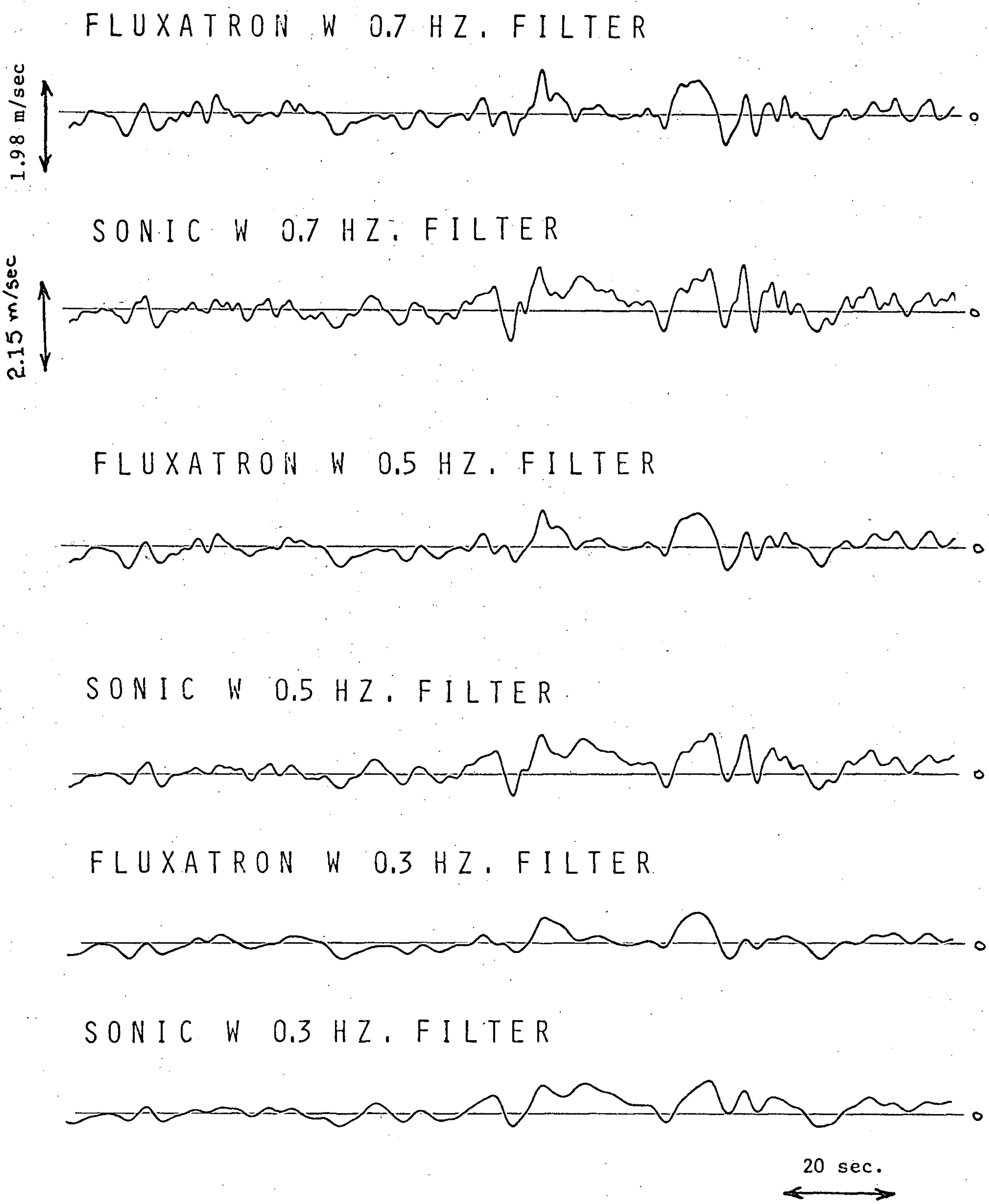
FLUXATRON W 0.7 HZ. FILTER
1.98 m/sec
SONIC W 0.7 HZ. FILTER
2.15 m/sec
FLUXATRON W 0.5 HZ. FILTER
SONIC W 0.5 HZ. FILTER
FLUXATRON W 0.3 HZ. FILTER
SONIC W 0.3 HZ. FILTER
0
20 sec.

FIGURE 21

pass filtering. At all stages there appeared to be stronger fluctuations associated with the SONIC W' than with the fluxatron. This indicated a significant loss of energy measurement by the fluxatron over the whole spectrum 0.3 hz. $\leq f \leq 10$ hz.

Figures 22, 23 and 24 show W' spectral computations for the three runs. The U.S.S.R. and U.B.C. sonic always agree closely for the full frequency range. The propeller W' spectra consistently falls below the sonic spectra especially in the high frequency area above $f = 2.0 \times 10^{-1}$ hz. The fact that the propeller absolute magnitude is still lower than both sonic measurements below $f = 2 \times 10^{-1}$ hz. illustrates the effect of the threshold and non-linear response features of Gill anemometers. A reduction in the energy measured at all frequencies was experienced by the Fluxatron as a total effect.

Table 3 shows estimates of the W'^2 cumulative integrals from the three runs. In the low frequency range 0.00055 hz. $< f < .158$ hz. the average ratio of cumulative integrals $\frac{(\text{FLUXATRON})}{(\text{SONIC(UBC)})}$ was about 0.745 indicating a loss of about 25% of the total energy in the FLUXATRON SIGNAL due to threshold and non-linear effects. This means that there would be an average amplitude loss of about 12% in the W' Gill signal below 0.158 hz. In the high frequency range where about 2/3 of the total fluctuation energy was to be found, (0.158 hz $< F <$ 10.8 hz.), the high frequency

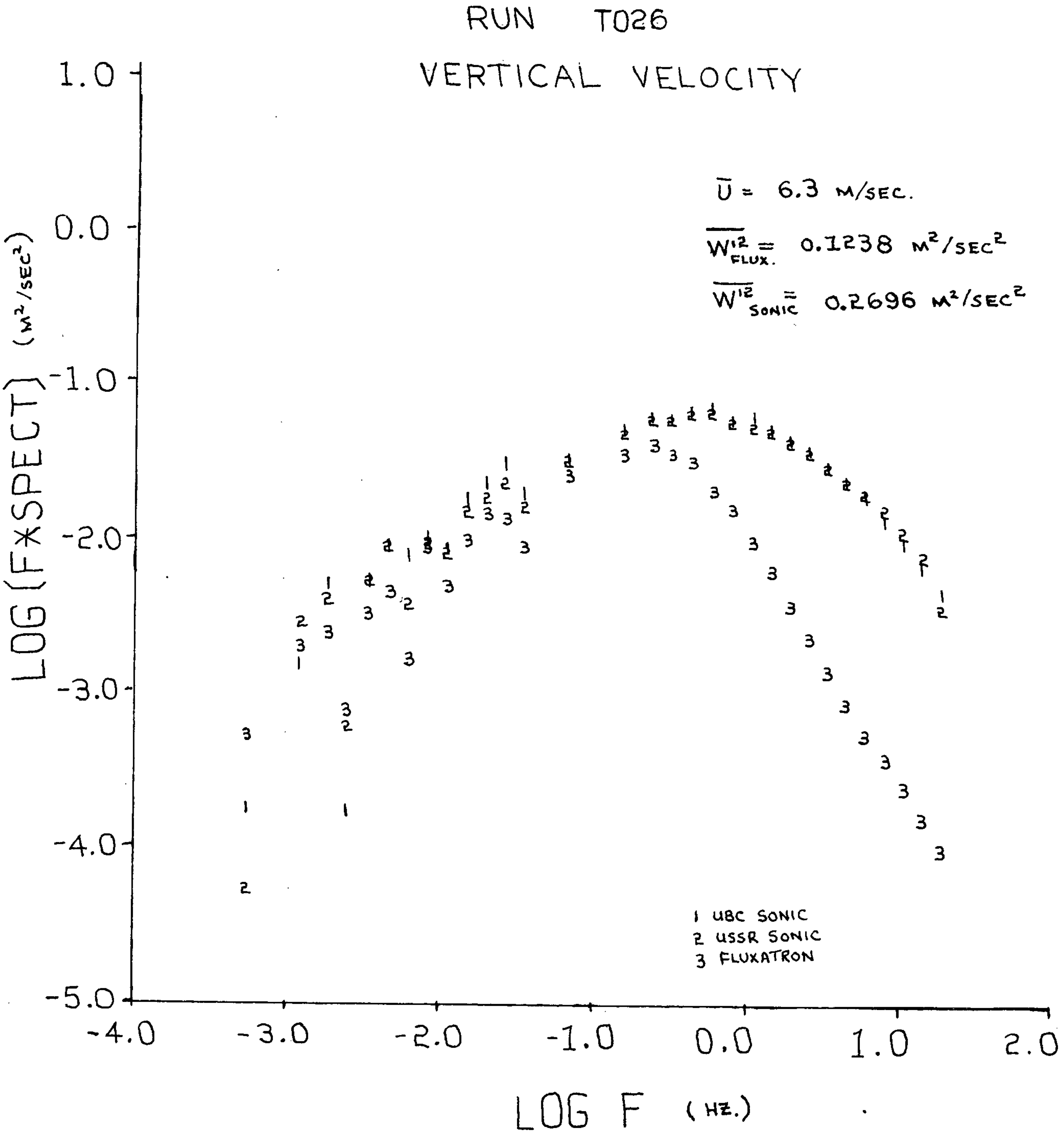
RUN T026
VERTICAL VELOCITY
$\bar{U}$ = 6.3 M/SEC.
$\overline{W'^2}_{FLUX.}$ = 0.1238 M^2/SEC^2
$\overline{W'^2}_{SONIC}$ = 0.2696 M^2/SEC^2
LOG{F*SPECT} (M^2/SEC^2)
1.0
0.0
-1.0
-2.0
-3.0
-4.0
-5.0
-4.0
-3.0
-2.0
-1.0
0.0
1.0
2.0
LOG F (HZ.)
1 UBC SONIC
2 USSR SONIC
3 FLUXATRON

FIGURE 23

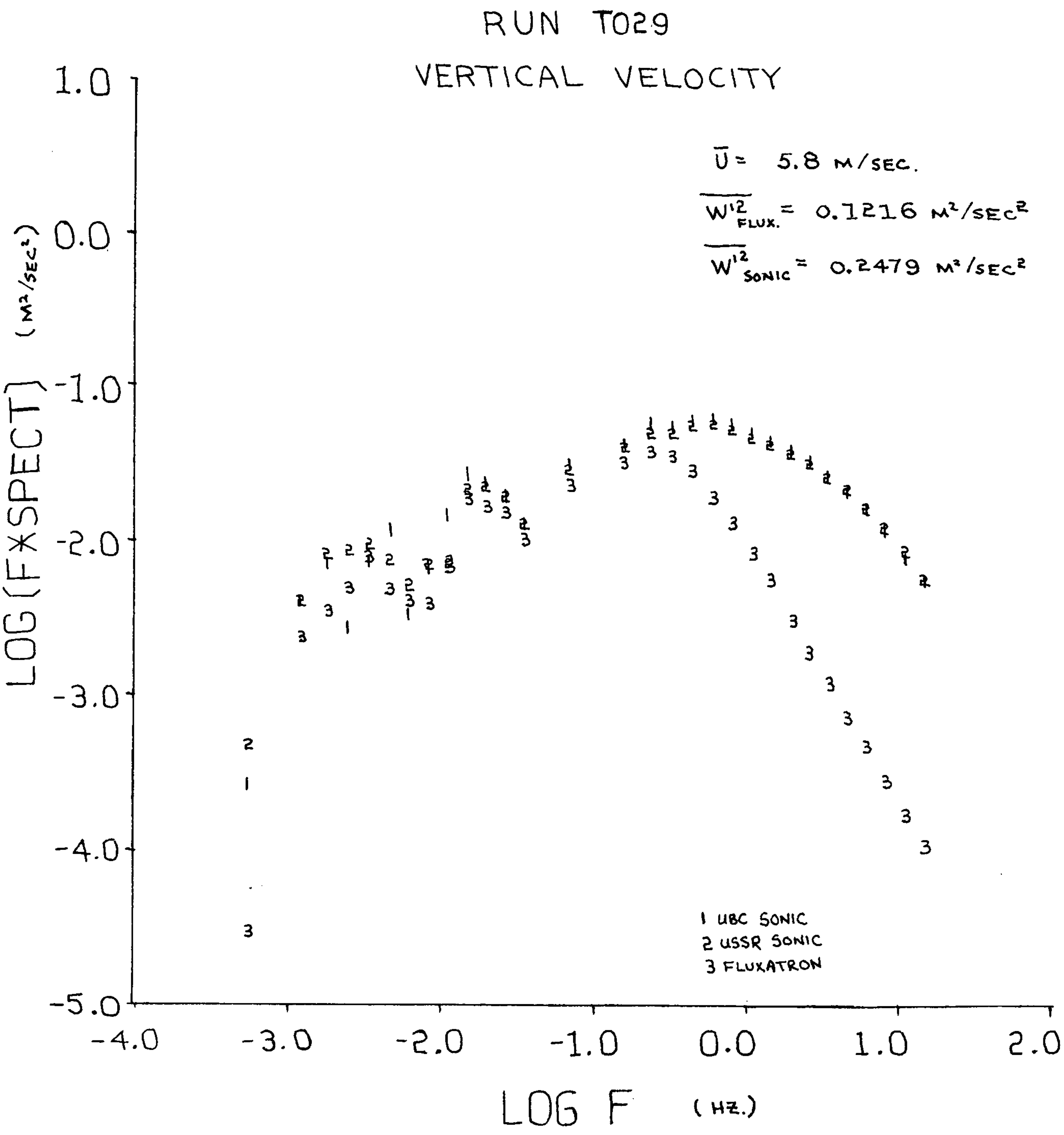
RUN T029
VERTICAL VELOCITY
$\bar{U}$ = 5.8 M/SEC.
$\overline{W'^2}_{FLUX.}$ = 0.7216 M^2/SEC^2
$\overline{W'^2}_{SONIC}$ = 0.2479 M^2/SEC^2
1 UBC SONIC
2 USSR SONIC
3 FLUXATRON
LOG(F*SPECT) (M^2/SEC^2)
LOG F (HZ.)
1.0
0.0
-1.0
-2.0
-3.0
-4.0
-5.0
-4.0
-3.0
-2.0
-1.0
0.0
1.0
2.0

FIGURE 24

TABLE 3

$\overline{w'w'}$ CUMULATIVE INTEGRALS

(M.K.S. UNITS)

.00055hz.< f <.158hz.

RUN	FLUXATRON	SONIC(UBC)	SONIC(USSR)	FLUX./SONIC(UBC)
T013	0.03601	0.0474	0.0506	0.760
T026	0.0533	0.0758	0.0713	0.703
T029	0.0581	0.0753	0.0725	0.771

.158hz.< f < 10.8hz.

RUN	FLUXATRON	SONIC(UBC)	SONIC(USSR)	FLUX./SONIC(UBC)
T013	0.04680	0.1272	0.1371	0.368
T026	0.0705	0.1938	0.1913	0.364
T029	0.0635	0.1726	0.1650	0.368

.00055hz.< f < 10.8hz.

RUN	FLUXATRON	SONIC(UBC)	SONIC(USSR)	FLUX./SONIC(UBC)
T013	0.08281	0.1746	0.1877	0.474
T026	0.1238	0.2696	0.2626	0.459
T029	0.1216	0.2479	0.2375	0.491

attenuation of the propeller also affected its results. In this range the average ratio of cumulative integrals $\frac{(\text{FLUXATRON})}{(\text{SONIC(UBC)})}$ was about 0.367 indicating about 63% of the propeller energy was lost due to its limited high frequency response. The overall result was a 0.475 ratio of W' cumulative integrals of FLUXATRON VS. SONIC for the entire frequency range studied. A total loss then of about 52% of the total fluctuating W' energy is experienced by the FLUXATRON.

Figures 25, 26 and 27 show ratios of the spectral estimates $\frac{(\text{W' GILL})}{(\text{W' SONIC})}$ for runs T013, T026 and T029 respectively. Below $f = 2 \times 10^{-1}$ hz. the agreement was about 0.75:1.0 except at lowest frequencies where the high pass filters in the Fluxatron (Dyer and Hicks, 1970) became significant (especially in Run T013) and where the signal sample time was small. In the higher frequency area, the GILL/SONIC ratio becomes half of the mean ratio at f = 0.70 hz., f = 0.60 hz., and f = 0.60 hz. respectively for the three runs. This would correspond to a Krohnhite filter with a cut-off frequency of near f = 3 hz. in the system. This result was visually observed in the study of the time traces. The random variation of the ratio from the mean in the mid-frequency range was probably a function of how much energy at each frequency was lost while in threshold or non-linear conditions during each run.

Figure 28 shows the joint probability density of W' SONIC across and W' FLUXATRON down. The contours

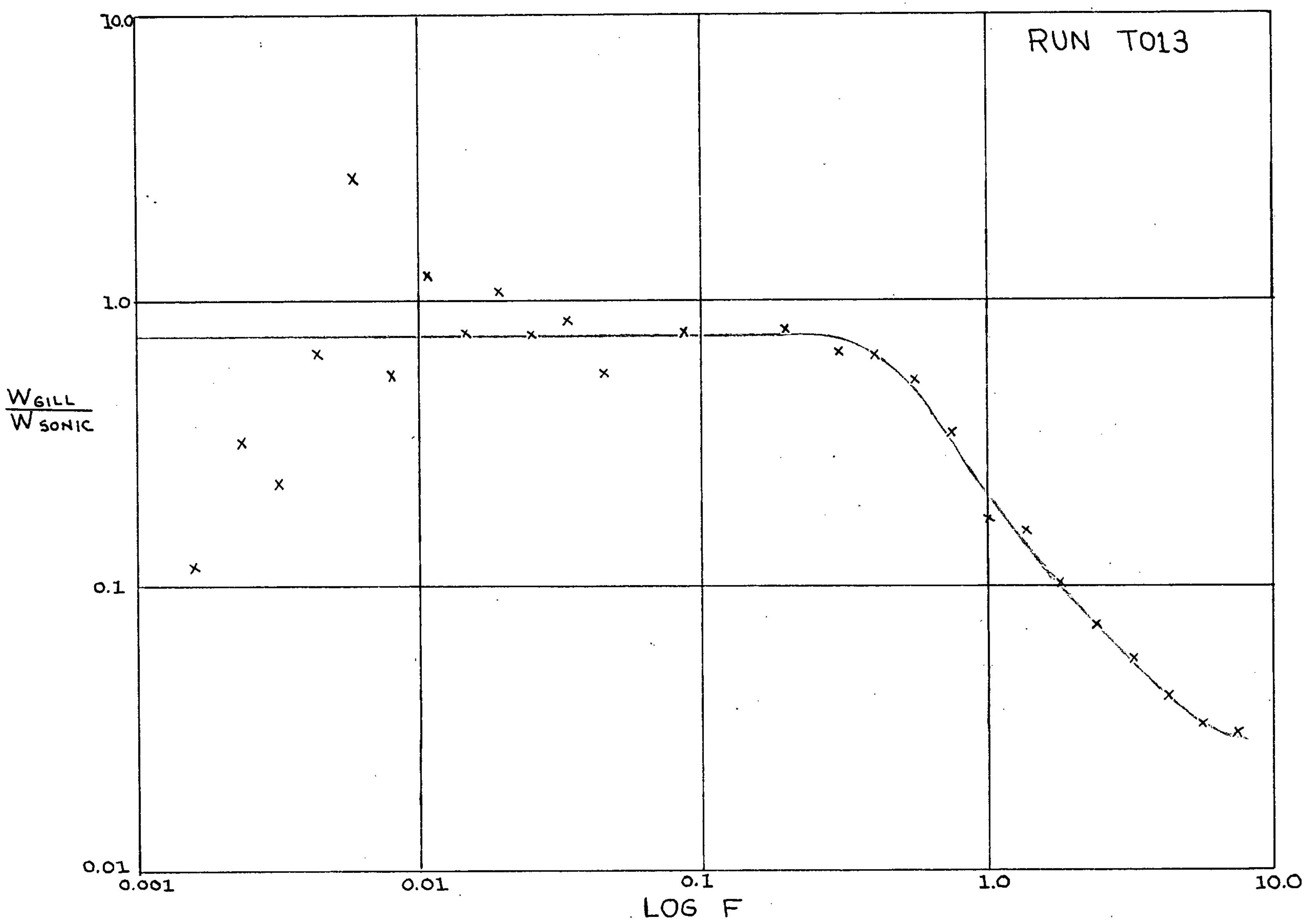

FIGURE 25 - RATIO OF SPECTRAL ESTIMATES

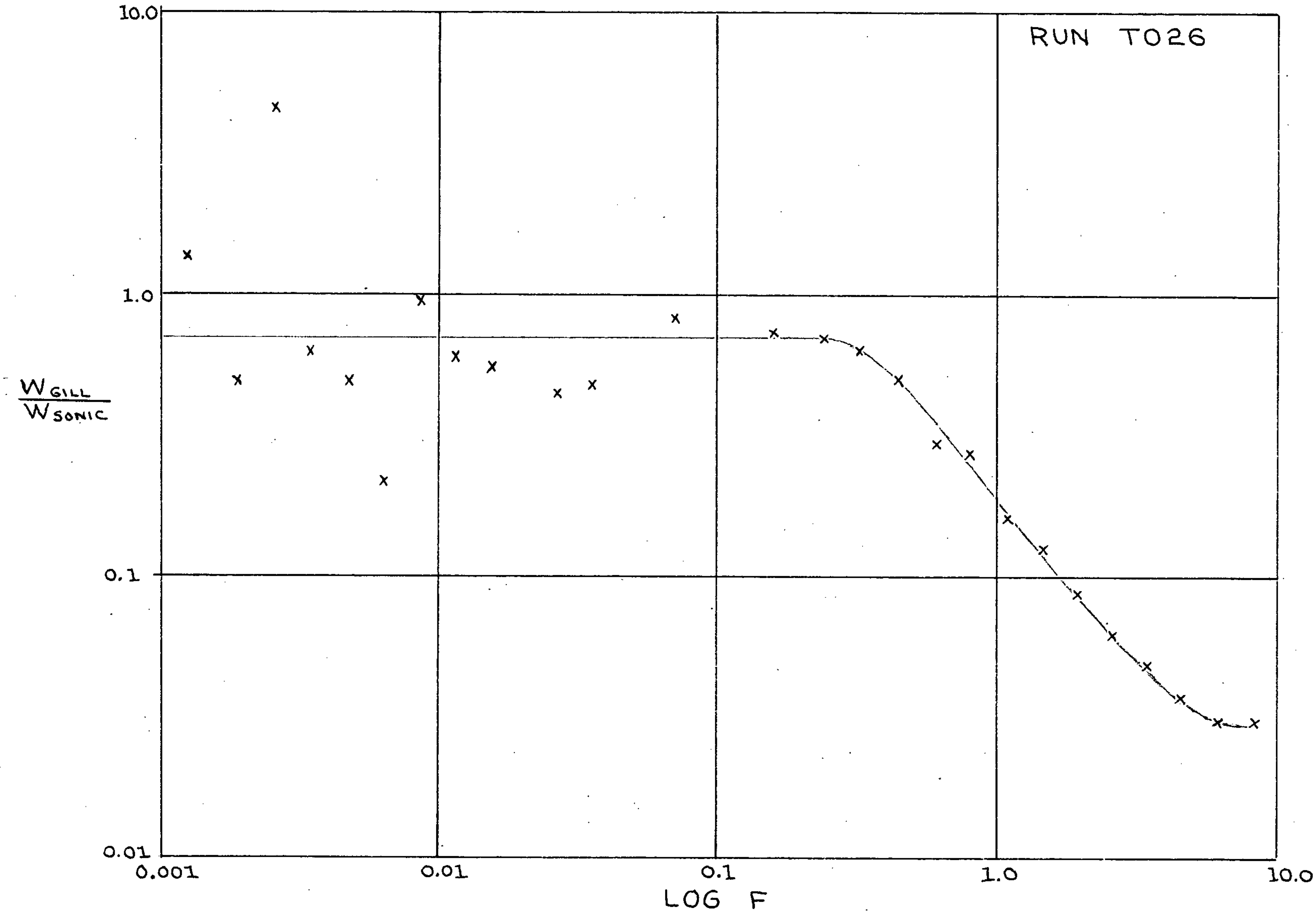

FIGURE 26 - RATIO OF SPECTRAL ESTIMATES

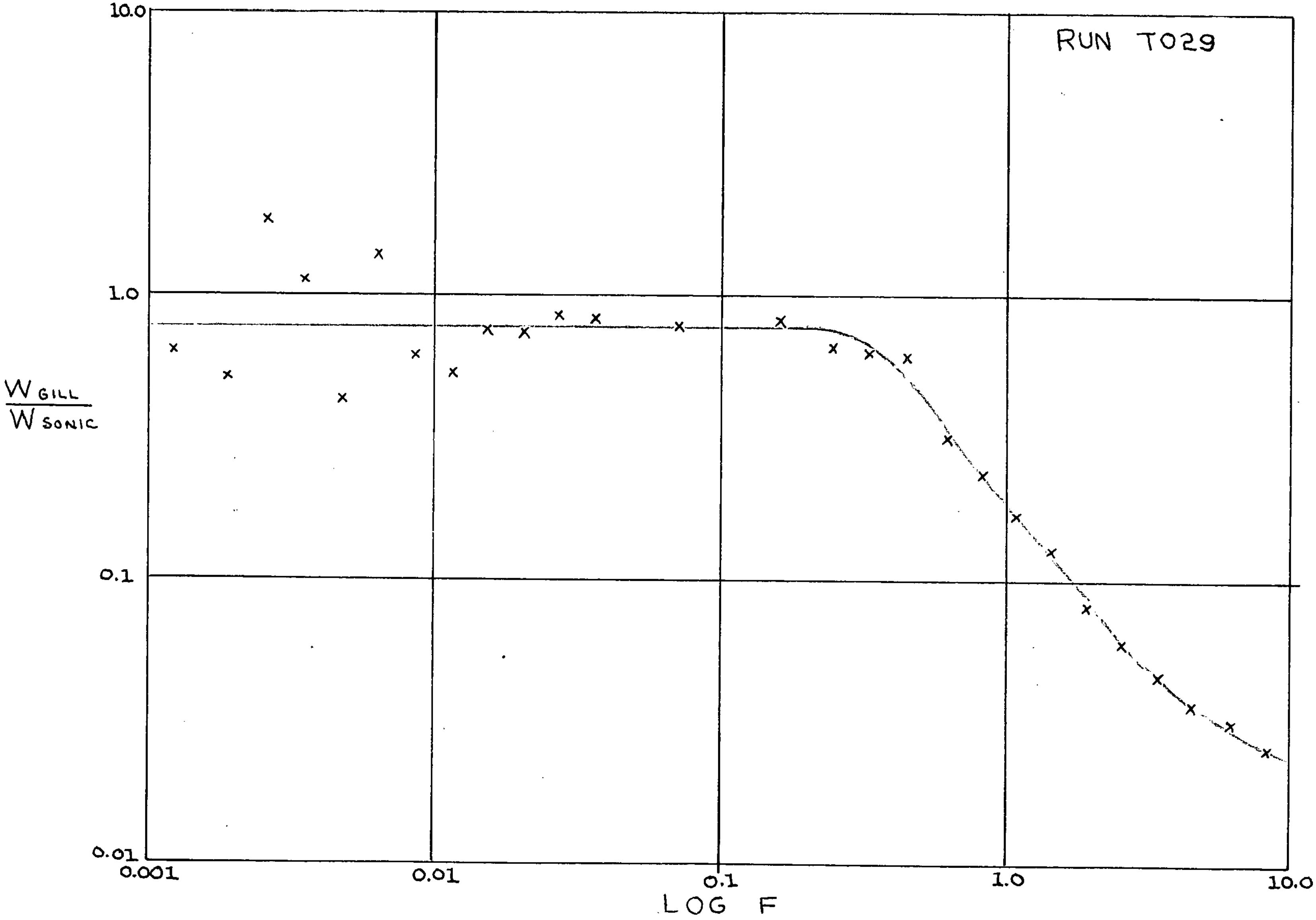

FIGURE 27 - RATIO OF SPECTRAL ESTIMATES

σW_{SONIC}

σW_{GILL}	-3.0	-2.5	-2.0	-1.5	-1.0	-0.5	0.0	0.5	1.0	1.5	2.0	2.5	3.0	3.5
-3.5	0	3	7	0	4	6	0	1	4	0	0	0	0	0
-3.0	0	23	21	19	27	13	3	4	5	0	0	0	0	0
-2.5	0	32	38	59	51	46	10	6	15	0	0	0	0	0
-2.0	0	13	51	97	103	176	122	85	74	16	6	6	7	0
-1.5	0	15	71	102	277	357	362	226	105	41	21	5	3	0
-1.0	0	13	50	114	513	784	794	505	333	80	28	14	7	3
-0.5	0	12	43	99	425	917	1019	1029	573	190	93	33	5	6
0.0	0	5	15	57	211	640	842	809	695	273	162	79	18	22
0.5	0	0	0	45	114	261	581	513	523	291	199	105	28	7
1.0	0	0	3	21	70	138	258	264	289	239	152	74	19	17
1.5	0	4	6	0	10	66	115	128	168	119	98	93	15	4
2.0	0	0	0	0	5	21	36	33	51	34	79	26	9	2
2.5	0	0	0	0	0	7	12	16	51	49	29	28	8	0
3.0	0	0	0	0	0	3	2	8	27	1	0	11	9	0
3.5														

NORMALIZED

FIGURE 28 - JOINT PROBABILITY DENSITY OF W GILL AND W SONIC

represent lines of constant density at intervals of 100. The ridge of highest density marked with a dotted line represents a best approximation of the two instrument responses. If both signals were exactly the same, a density distribution would show a straight line of slope 1 through the centre. The fact is that they are not the same. The dotted line in fact follows very closely the hypothesized response outlined in Figure 6. The zero level of the FLUXATRON'S propeller was offset -0.25 in recording which explains the vertical offset on the graph. It would appear that a threshold area was observed between $\pm$ 0.6 volts on the sonic scale and a non-linear range out to about -1.5 volts. There was a much larger spread in the results than for the U' measurements indicating a smaller correlation between the W' signals than for U' signals.

Figure 29 shows the probability distribution of the W' signals for Run T029. The Gill shows a higher probability of finding no fluctuations than does the sonic. Also it would appear for this observation that the distribution of the sonic W' is non-gaussian in the positive (updraft region) especially. A check with another independent means for calculating the probability distribution revealed the same fact. Figure 30 shows the probability distribution for all 32 minutes of Run T029.

Figure 31 shows a plot of the coherence and phase for the Fluxatron W' and Sonic (U.B.C.) W' signals for

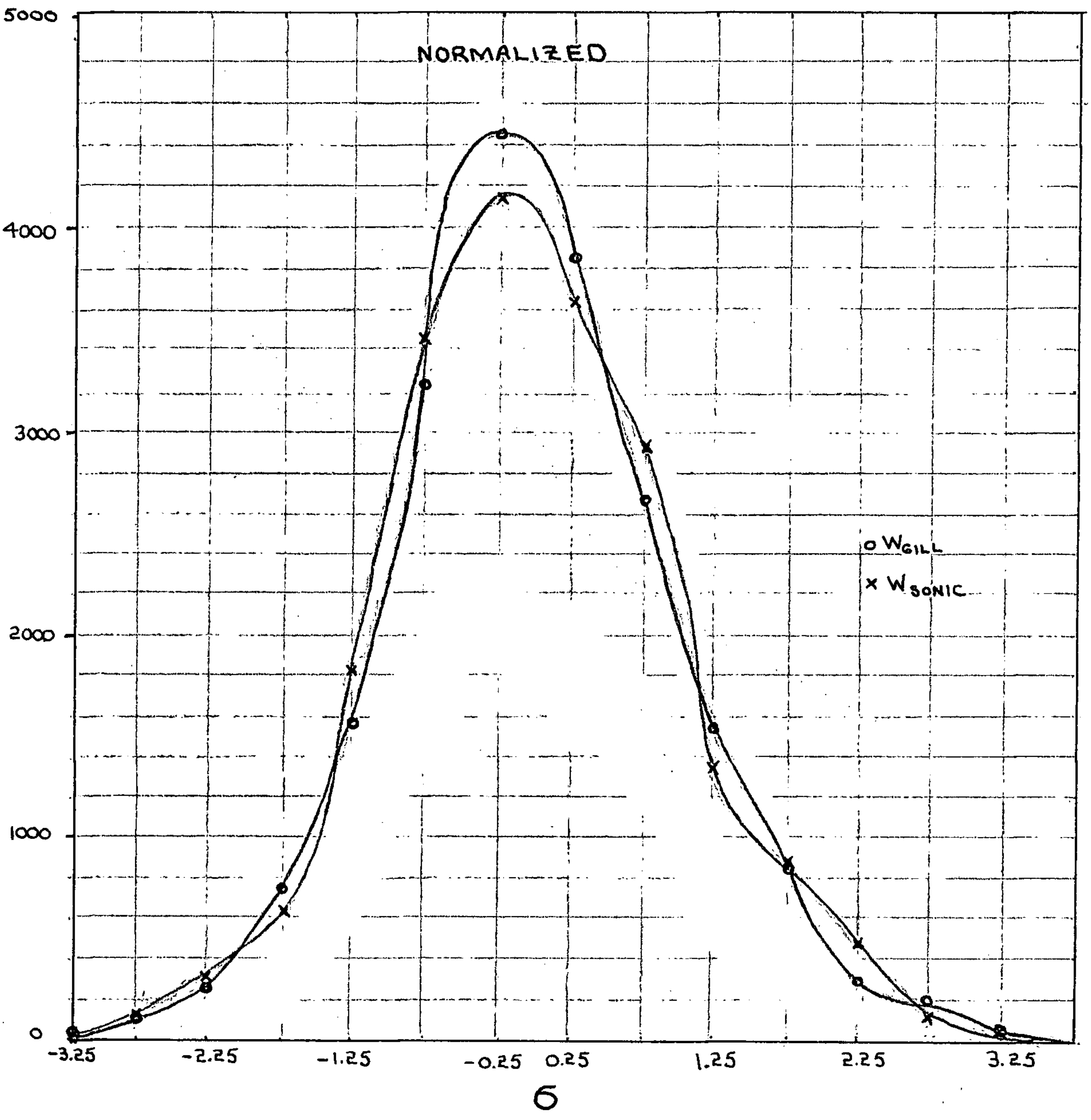

FIGURE #29 - PROBABILITY DISTRIBUTION OF W GILL AND W SONIC

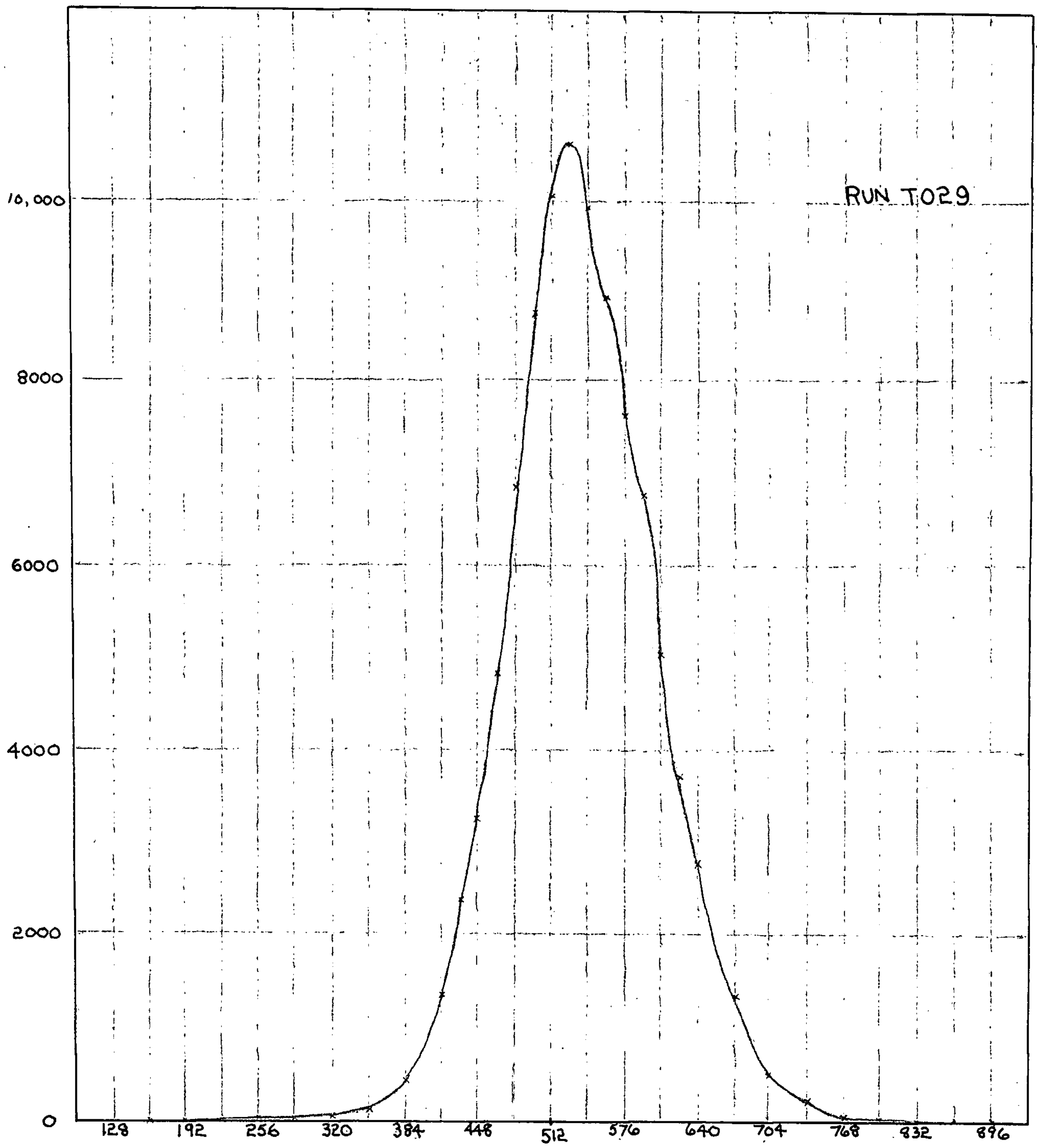

FIGURE 30 - TVERIF PROBABILITY DISTRIBUTION OF SONIC W

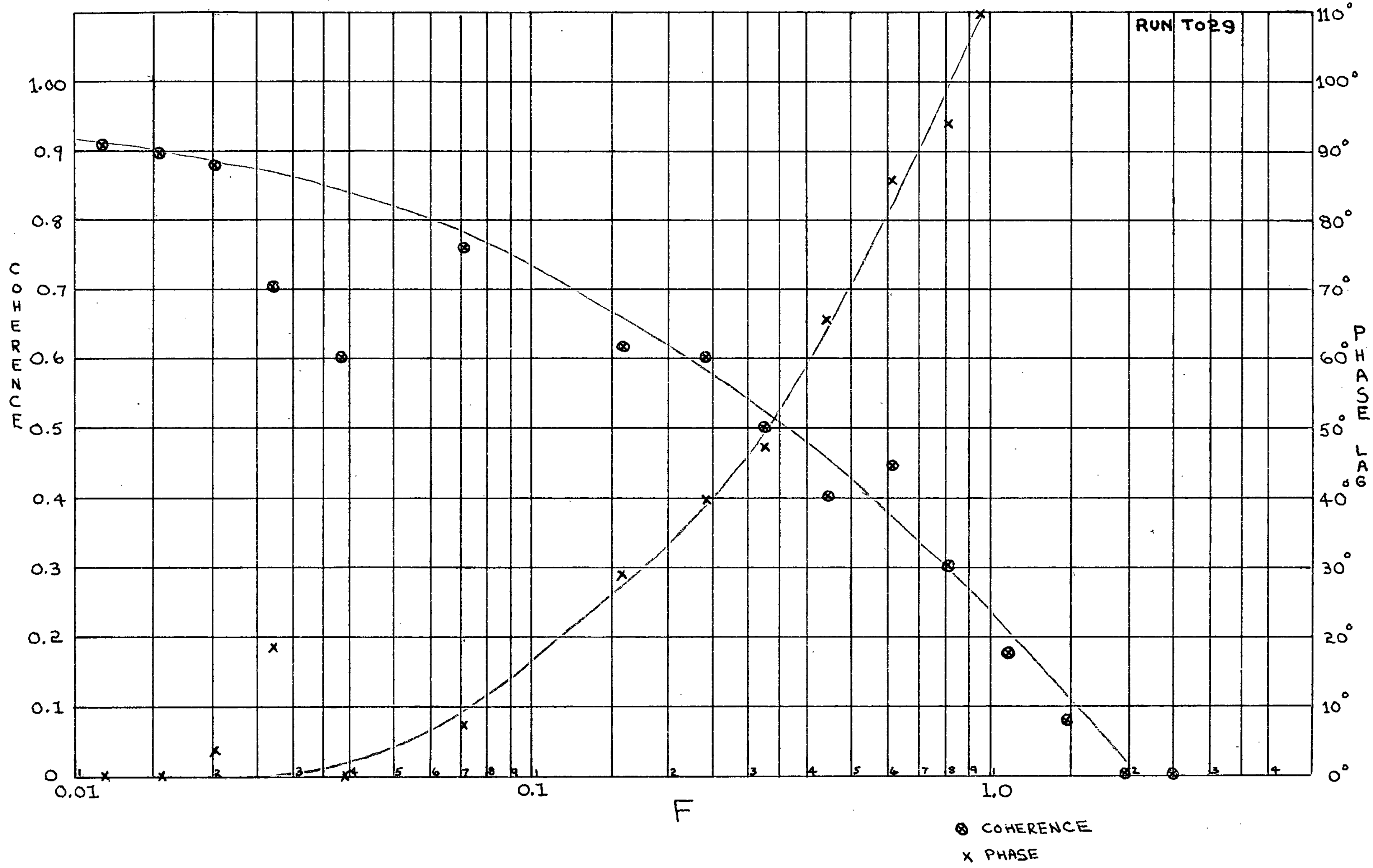

RUN TO29
COHERENCE
PHASE LAG
F
1.00
0.9
0.8
0.7
0.6
0.5
0.4
0.3
0.2
0.1
0
0.01
0.1
1.0
110°
100°
90°
80°
70°
60°
50°
40°
30°
20°
10°
0°
⊗ COHERENCE
x PHASE

FIGURE · 31

Run T029. The coherence was about 0.91 at f = 0.01 hz. and had fallen off to 0.5 by about f = 0.3 hz. The phase lag of the propeller was near zero at low frequencies and began to increase by f = 0.04 hz. At f = 0.3 hz. the phase lag was about 45°. According to specs, then, this corresponded to a Krnhbte frequency cut-off of about 1 hz.

3.2.3 Measurements of Momentum Flux

Figures 32, 33 and 34 show the cospectra of U'W' as calculated for RUNS T013, T026 and T029. The integral of the area under the cospectra is the kinematic momentum flux. The cospectral shapes and magnitudes were almost identical for the two sonic anemometers and very similar in shape to momentum cospectra measured in 1969 at Ladner, B.C. (McBean, 1970). However, the fluxatron cospectra were reduced in both shape and magnitude at higher frequencies.

Table 4 lists values of the U'W' cumulative integrals for the different frequency ranges. In the high frequency range (f > .158 hz.) where about 1/3 of the momentum flux was found the FLUXATRON was observed to have measured only about 50% of the total flux available. This was a result of the upper frequency limitations of the propeller. In the low frequency range (f > .158 hz.) where the other 2/3 of the momentum flux was found the FLUXATRON missed only about 25% of the total flux available. There was a large scatter in the spectral points, however, probably due to the non-linear response of the W' signals.

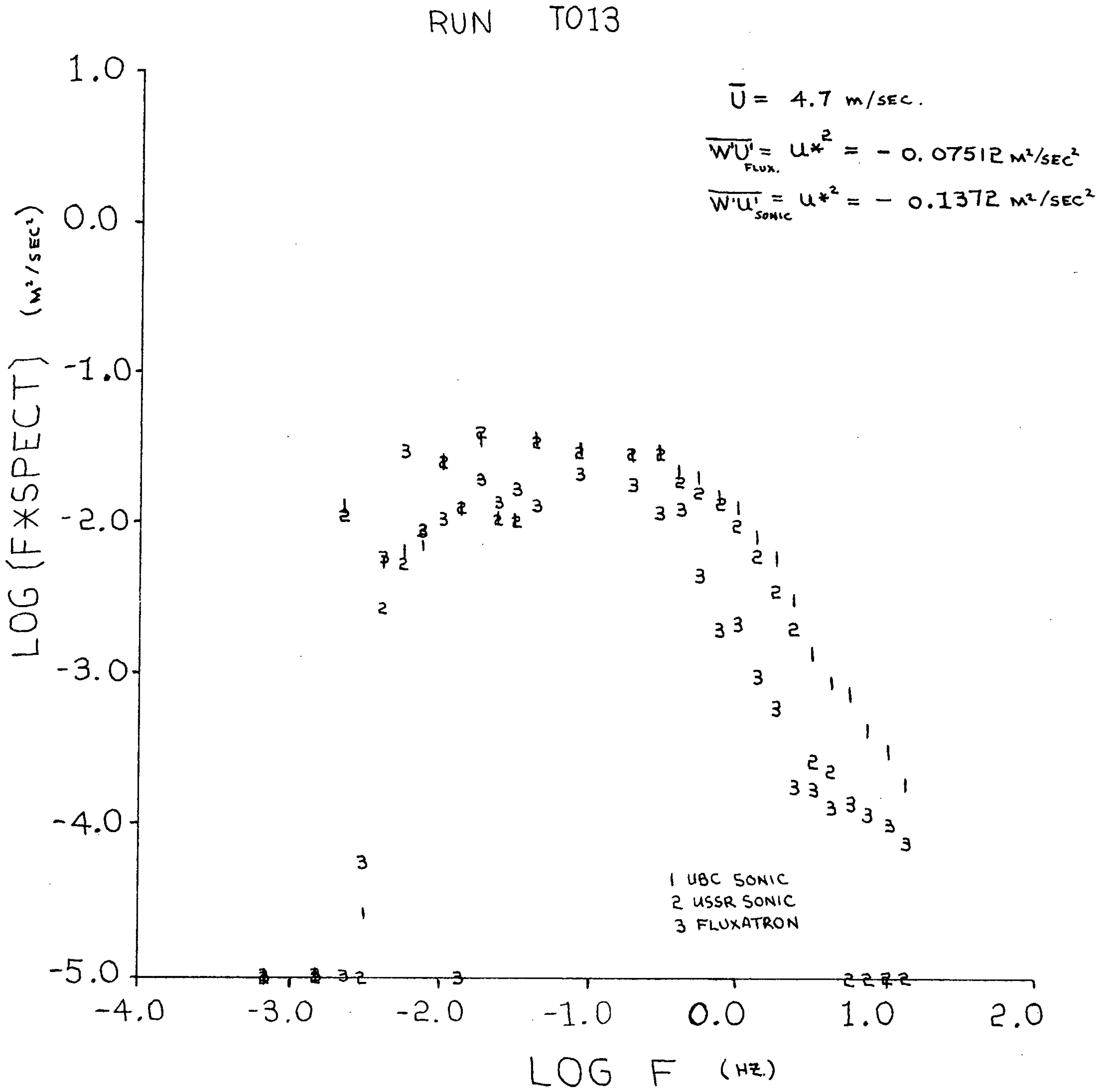

FIGURE 32 - U'W' COSPECTRA - RUN T013

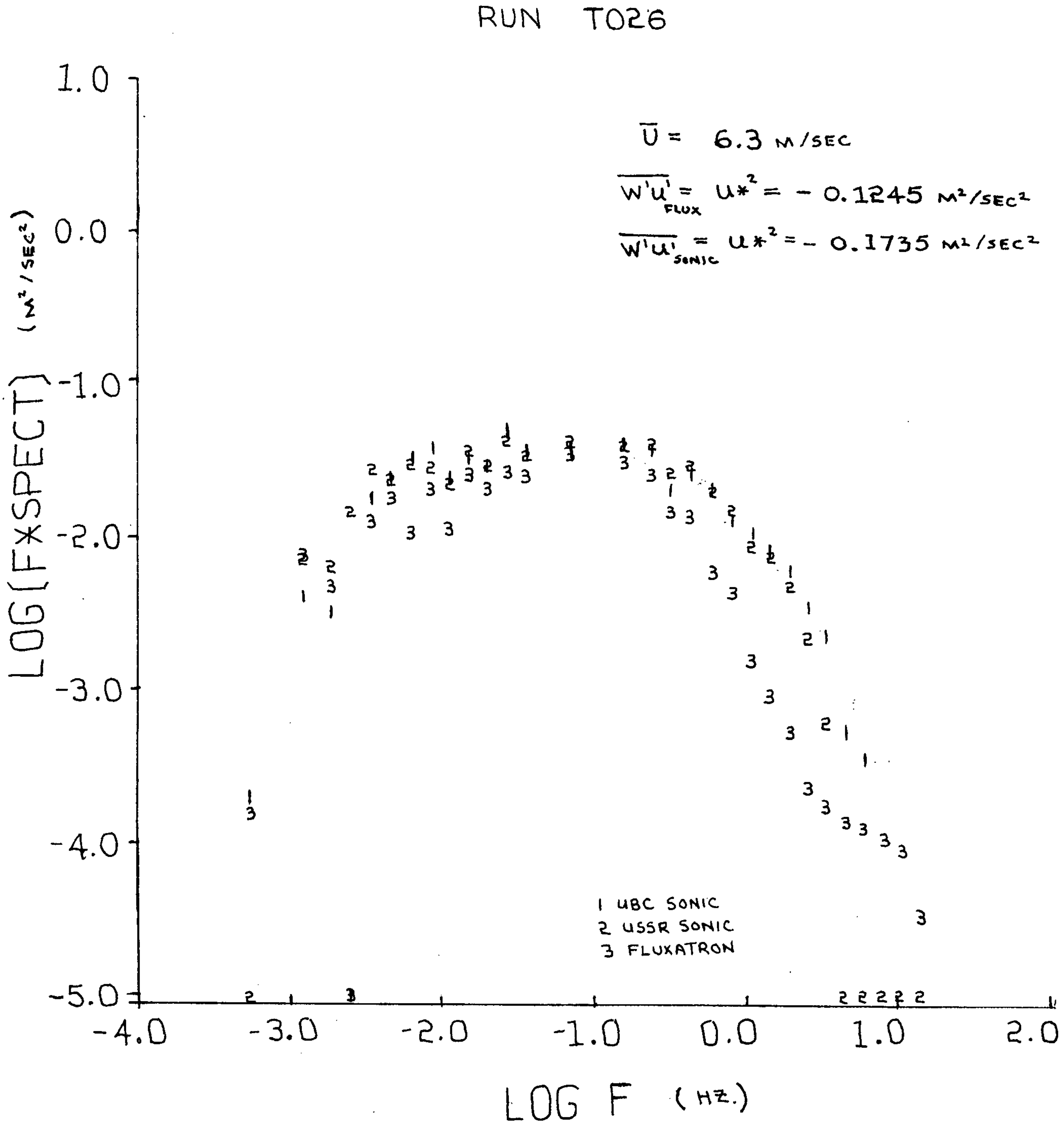

FIGURE 33 - U'W' COSPECTRA

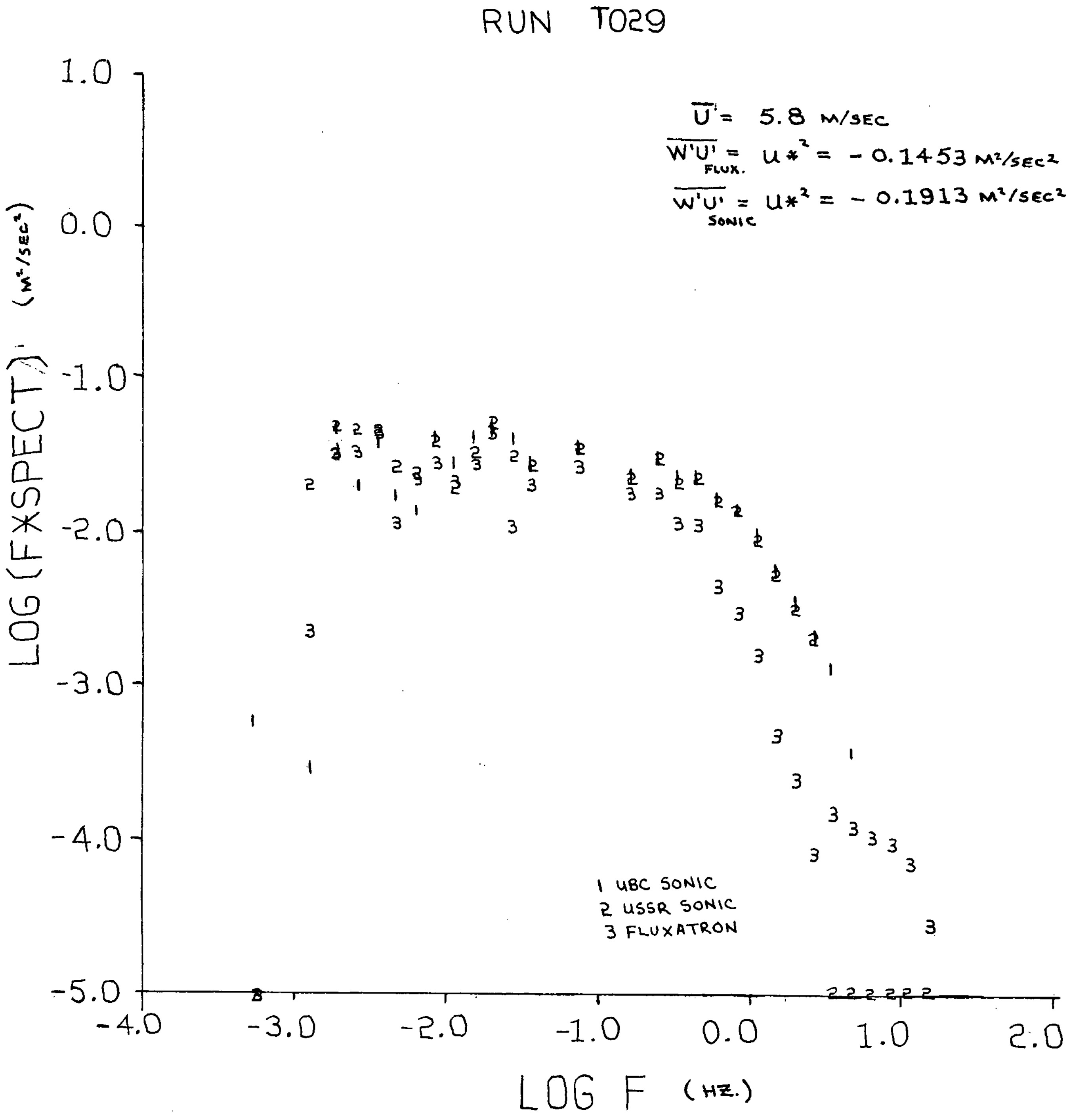

FIGURE 34 - U'W' COSPECTRA

TABLE 4

U'W' CUMULATIVE INTEGRALS

(M.K.S. UNITS)

.00055hz.< f <.158hz.

RUN	FLUXATRON	SONIC(UBC)	SONIC(USSR)	FLUX./SONIC(UBC)
T013	-0.05409	-0.0843	-0.0756	0.642
T026	-0.0890	-0.1145	-0.1372	0.778
T029	-0.1207	-0.1410	-0.1630	0.855

.158hz.< f < 10.8hz.

RUN	FLUXATRON	SONIC(UBC)	SONIC(USSR)	FLUX./SONIC(UBC)
T013	-0.02103	-0.0529	-0.0451	0.398
T026	-0.0355	-0.0591	-0.0657	0.601
T029	-0.0246	-0.0503	-0.0464	0.489

.00055hz.< f < 10.8hz.

RUN	FLUXATRON	SONIC(UBC)	SONIC(USSR)	FLUX./SONIC(UBC)
T013	-0.07512	-0.1372	-0.1207	0.548
T026	-0.1245	-0.1735	-0.2029	0.717
T029	-0.1453	-0.1913	-0.2094	0.760

The overall effect was a reduced momentum flux measurement of about 0.675 for the Fluxatron when compared to a sonic type anemometer. Individual ratios of the flux measurements by FLUXATRON VS. THE U.B.C. sonic were 0.548, 0.717 and 0.760 for the three runs T013, T026 and T029 respectively.

It must be noted that Run T013 was taken in the evening under more stable conditions than were T026 and T029. The average ratio of $\frac{\overline{U'W'}\,\mathrm{FLUX}}{\overline{U'W'}\,\mathrm{SONIC}}$ for the two unstable cases would be 0.739.

Figures 35, 36 and 37 show ratios of the cospectral estimates $\frac{(\overline{U'W'}\ \mathrm{Gill})}{(\overline{U'W'}\,\mathrm{Sonic})}$ for Runs T013, T026 and T029. The stable case (RUN T013) showed much more spread especially in the low frequency region than did the more unstable cases, T026 and T029.

Table 5 shows some calculations of the drag coefficient c_d and the correlation coefficient Γ_{wu} for the FLUXATRON and two sonic anemometers.

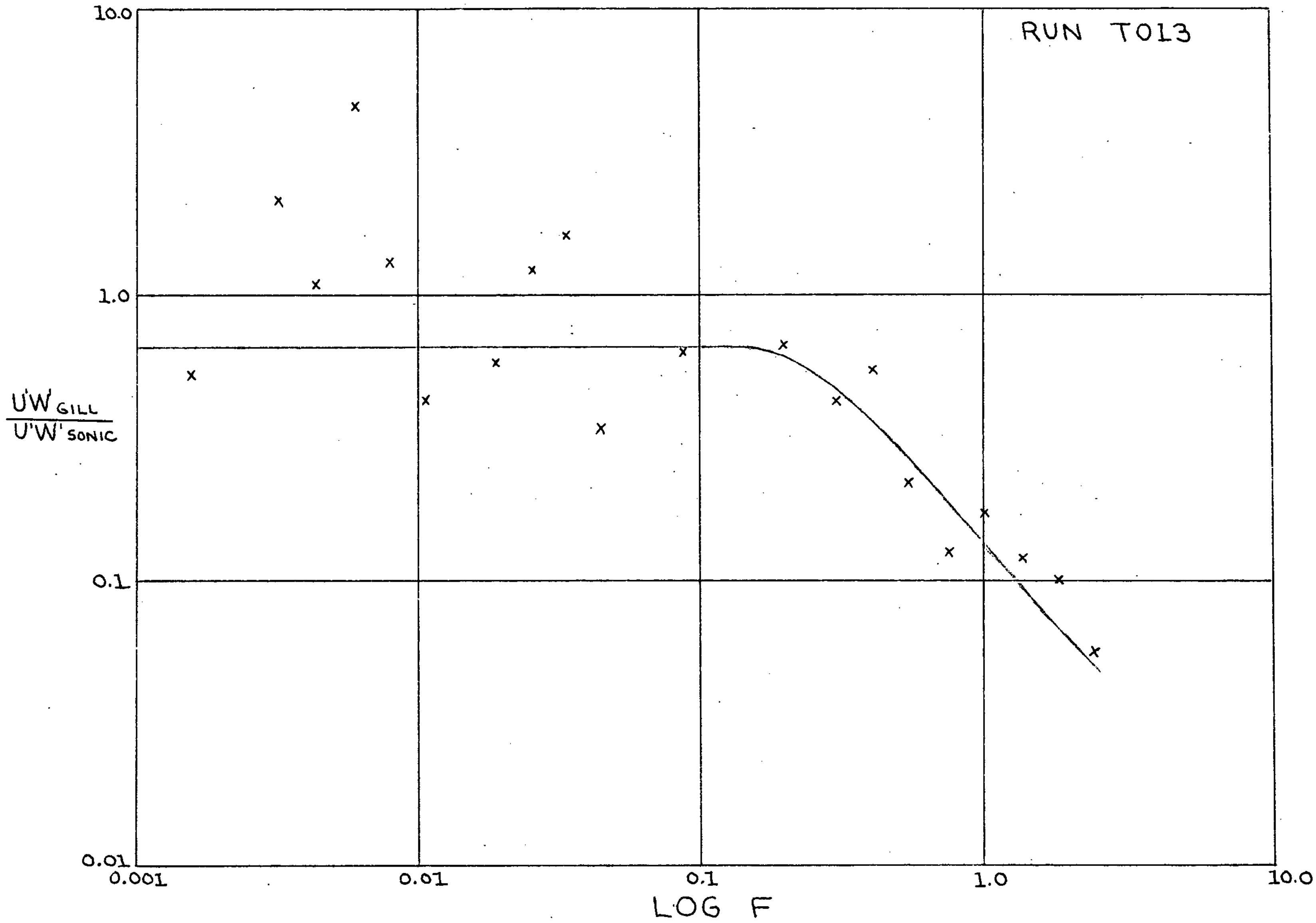

FIGURE 35 - RATIO OF SPECTRAL ESTIMATES

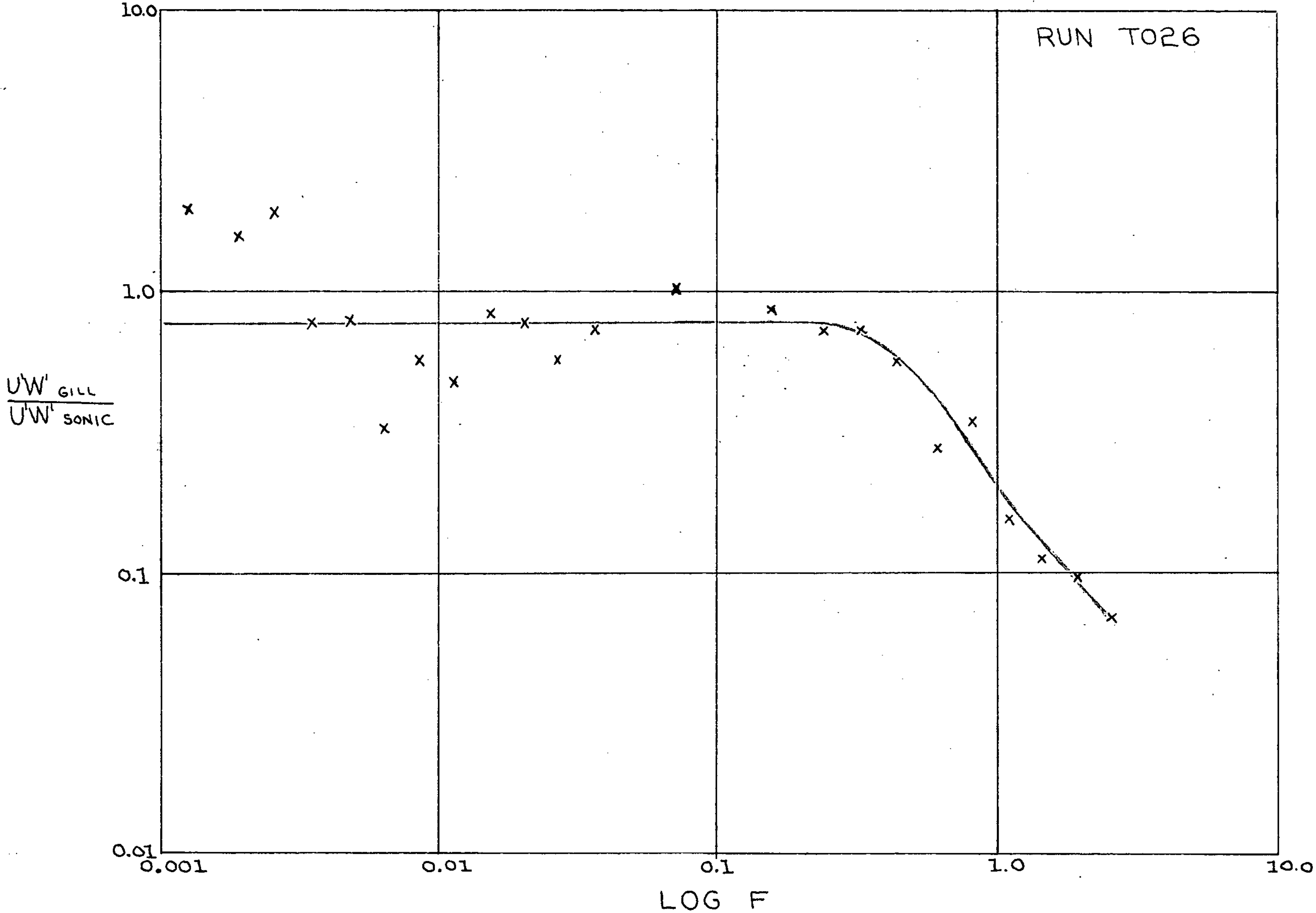

FIGURE 36 - RATIO OF SPECTRAL ESTIMATES

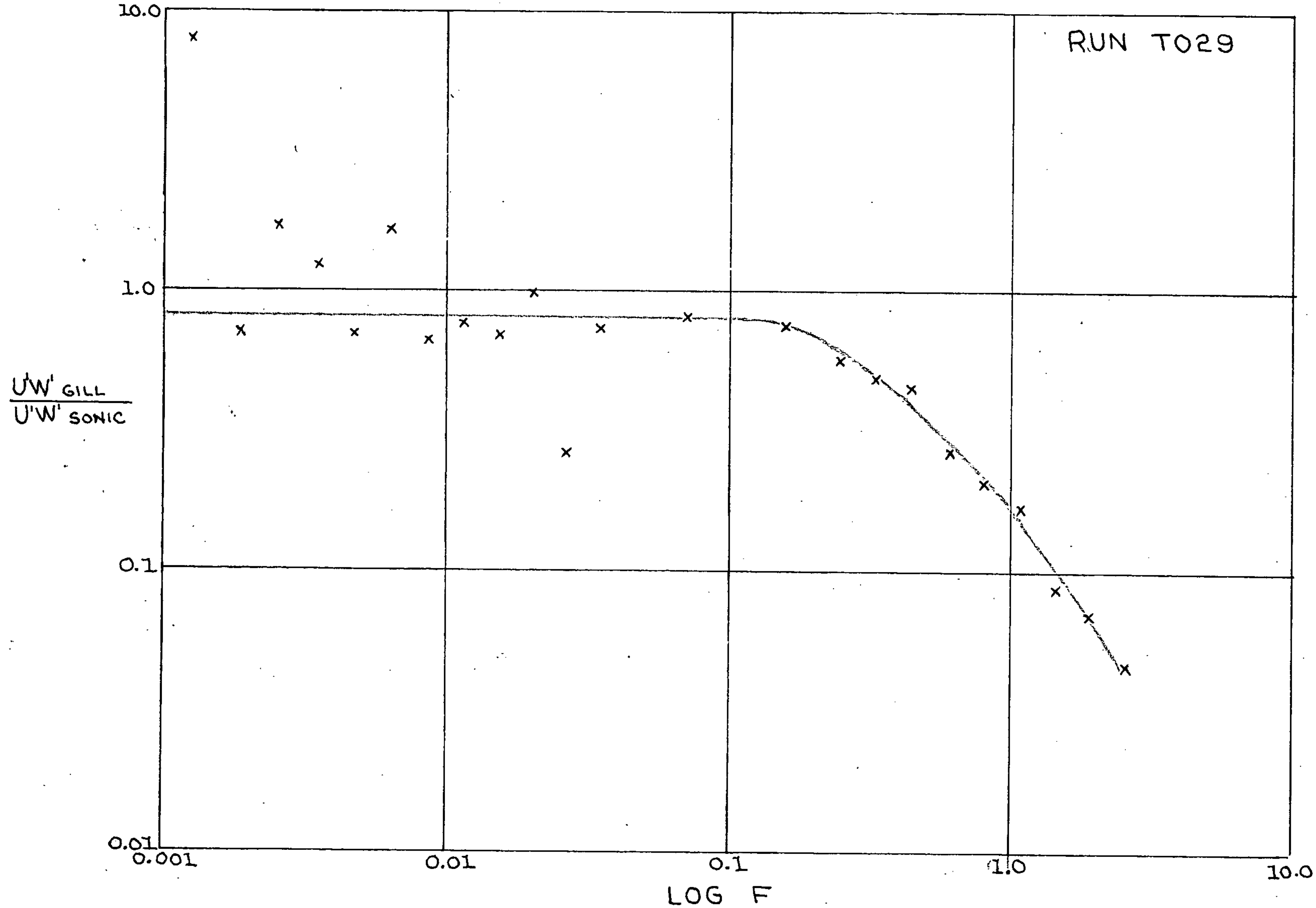

FIGURE 37 - RATIO OF SPECTRAL ESTIMATES

TABLE 5

CALCULATIONS OF Γ_{WU} AND C_D

(M.K.S. UNITS)

$\Gamma_{WU} = U*^2/(\text{sigma } U)(\text{sigma } w)$

RUN	FLUXATRON	SONIC(UBC)	SONIC(USSR)
T013	0.286	0.379	0.331
T026	0.353	0.337	0.394
T029	0.353	0.344	0.377

$C_D = U*^2/\bar{U}^2$

RUN	FLUXATRON	SONIC(UBC)	SONIC(USSR)
T013	0.00348	0.00635	0.00558
T026	0.00314	0.00437	0.00511
T029	0.00432	0.00569	0.00622

CHAPTER 4

CONCLUSIONS

The turbulent horizontal and vertical components of the wind were measured and compared using a sonic-type anemometer and Gill propellers.

Measurements of the horizontal velocity fluctuations showed good agreement between sonics and propeller in both the time domain and frequency domain. Best shape agreement in the time traces occured when frequencies $f > 6$ hz. had been removed by the Krohnhite filter from Sonic U' ($f_c = 1.4$ hz.). This meant the propeller had an associated distant constant of about 4 metre considering the mean wind at the time. Spectral computations revealed the Fluxatron in general tended to overestimate the total U' variance by about 20% for frequencies below f = 0.2 hz. indicating a possible calibration discrepancy. By looking at where the ratio of the power spectral estimates (propeller vs. sonic) fell to about 0.50 it was possible to reconfirm the value of the distant constant for the propeller. The average for the three runs was 6.90 metres. The joint probability density of U' sonic and U' Gill confirmed the linear response of the U' Gill propeller.

Measurements of the vertical velocity fluctuations showed poorer agreement between sonic and propeller in both the time and frequency domains. Time traces of sonic W' and propeller W' showed best agreement when a 3hz. Krohnhite filter was used on the Sonic W' (f_c=0.9hz.). By filtering both propeller and sonic signals for 0.2 hz. < f < 10 hz. a significant loss of propeller energy measurement was observed over the full range of frequency. Spectral computations showed also that the W' fluctuating energy of the propeller was always less than that from the sonics. Non-linear and threshold effects were alleged to have caused an average 25% reduction of the total W' energy measured by the propeller in the frequency region f < 0.158 hz. The propeller's high frequency cut-off at $f_c \doteq 0.9$ hz. and its non-linear response at low wind speeds then resulted in a total loss of 52% of W' fluctuating energy over the full frequency range studied. The joint probability density distribution again confirmed the non-linear response of the W' propeller and indicated a non-gaussian distribution even for the sonic W'.

Analysis of the cospectra of U'W' showed that significant contributions to the momentum flux were to be found in the frequency domain 0.001 hz. < f < 5.0 hz. Below f = 0.158 hz. the non-linear response and stalling effects in the W' propeller signal were the probable reasons for the average ratio of ($\overline{U'W'\text{ Gill}}$ / $\overline{U'W'\text{ sonic}}$) being 0.76. Above f = 0.158 hz. the high frequency losses of both the Gill U' and W' signals helped attenuate its U'W' cospectra more quickly than that for the sonics resulting in a measured loss of momentum flux. The combined response effects of the propeller were enough to reduce the Fluxatron's estimate of the total momentum flux by 32.5%.

Both sonic types of anemometers agreed closely as to shapes and absolute magnitudes of the spectra and co-spectra of U' and W'.

In the field, one method of minimizing the non-linearity and threshold effects at low vertical wind speeds would be to tilt the vertical sensor into the wind by 40°, or so, to always keep the propeller moving in one direction. This would assume the mean wind $\overline{U}$ near 5.0 m/sec. It could be mounted on the same assembly as the horizontal Gill so as to always face the mean wind.

REFERENCES

Bovsherov, V.M. and V.P. Voronov, 1960, 'Acoustic Wind Vane', Izv. Acad. of Sci. U.S.S.R., Geophys. Series, No. 6.

Dyer, A.J., B.B. Hicks and K.M. King, 1967, The Fluxatron - A Revised Approach to the Measurement of Eddy Fluxes in the Lower Atmosphere, Journal Appl. Meterorol., 6, 408-413.

Dyer, A.J. and B.B. Hicks, 1970, The Spatial Variability of Eddy Fluxes in the Constant Flux Layer, Quart. J. Roy. Meteorol. Soc., In press.

Hicks, B.B., 1970, The Measurement of Atmospheric Fluxes Near the Surface: A Generalized Approach, J. Appl. Meteorol., 9, 386-388.

McBean, G.A., 1970, The Turbulent Transfer Mechanisms in the Atmospheric Surface Layer. Ph.D. Thesis, University of British Columbia.

Mitsuta, Y., M. Miyake and Y. Kobovi, 1967, Three dimensional sonic anemometer-thermometer for atmospheric turbulence measurements. Kyoto Univ. Intern. Rep., 10 pp.

Miyake, M., M. Donelan, G. McBean, C. Paulsen, F. Badgley, and E. Leavitt, 1970, Comparison of Turbulent Fluxes over Water Determined by Profile and Eddy-correlation Techniques. Quart. J. Roy. Meteor. Soc., 96, pp. 132-137.

Tsvang, L.R., B.M. Koprov, O.A. Kuznetzov, M. Miyake, R.W. Stewart, and R.W. Burling, 1971, Comparison of Acoustic Instruments in Atmospheric Turbulence over Water. Boundary-Layer Meteorology, Vol. 2-2, 20-37.